

## RESEARCH ARTICLE

# STAU2 binds a complex RNA cargo that changes temporally with production of diverse intermediate progenitor cells during mouse corticogenesis

Rebecca Chowdhury<sup>1</sup>, Yue Wang<sup>1</sup>, Melissa Campbell<sup>1</sup>, Susan K. Goderie<sup>1</sup>, Francis Doyle<sup>2</sup>, Scott A. Tenenbaum<sup>2</sup>, Gretchen Kusek<sup>1</sup>, Thomas R. Kiehl<sup>1</sup>, Suraiya A. Ansari<sup>3,\*</sup>, Nathan C. Boles<sup>1,\*</sup> and Sally Temple<sup>1,\*,†</sup>

## ABSTRACT

STAU2 is a double-stranded RNA-binding protein enriched in the nervous system. During asymmetric divisions in the developing mouse cortex, STAU2 preferentially distributes into the intermediate progenitor cell (IPC), delivering RNA molecules that can impact IPC behavior. Corticogenesis occurs on a precise time schedule, raising the hypothesis that the cargo STAU2 delivers into IPCs changes over time. To test this, we combine RNA-immunoprecipitation with sequencing (RIP-seq) over four stages of mouse cortical development, generating a comprehensive cargo profile for STAU2. A subset of the cargo was 'stable', present at all stages, and involved in chromosome organization, macromolecule localization, translation and DNA repair. Another subset was 'dynamic', changing with cortical stage, and involved in neurogenesis, cell projection organization, neurite outgrowth, and included cortical layer markers. Notably, the dynamic STAU2 cargo included determinants of IPC versus neuronal fates and genes contributing to abnormal corticogenesis. Knockdown of one STAU2 target, *Taf13*, previously linked to microcephaly and impaired myelination, reduced oligodendrogenesis *in vitro*. We conclude that STAU2 contributes to the timing of corticogenesis by binding and delivering complex and temporally regulated RNA cargo into IPCs.

**KEY WORDS:** RNA-binding protein, STAU2, RIP-seq, Cerebral cortex, Mouse, Intermediate progenitor cells

## INTRODUCTION

During mouse corticogenesis, radial glial cells (RGCs), the principal progenitor cells in the cerebral cortex, can divide asymmetrically in the ventricular zone (VZ) to produce intermediate progenitor cells (IPCs) (Götz and Barde, 2005; Sessa et al., 2008). IPCs move to the subventricular zone (SVZ) where they produce small cohorts of neurons that migrate to the developing cortical plate (CP) (Haubensak et al., 2004; Miyata et al., 2004; Noctor et al., 2004).

Differently specified IPCs play a central role in corticogenesis. Neurons of different layers are produced in temporal order (Hevner et al., 2003), with early IPCs generating all subtypes of cortical projection neurons, and later IPCs producing neurons of more superficial layers (Kowalczyk et al., 2009; Mihalas et al., 2016; Vasistha et al., 2015). In late embryogenesis, after neurogenesis is complete, progenitors produce astrocytes and oligodendrocytes, which populate the developing cortex (Kriegstein and Alvarez-Buylla, 2009; Noctor et al., 2008).

Mouse cortical lineage trees (Qian et al., 1998; Shen et al., 2006) resemble those of *Drosophila*, where neuroblasts undergo repeated asymmetric divisions to produce temporally specified ganglion mother cells (GMCs), which then produce cohorts of different types of neurons. Several molecules are asymmetrically inherited during *Drosophila* neuroblast divisions that act as determinants of the GMC fate. Staufin, a double-stranded RNA-binding protein (dsRBP), is distributed asymmetrically into the GMC carrying RNA cargo molecules that impact differentiation, for example, the *prospero* transcript (Broadus et al., 1998).

In mammals, two Staufin genes are present: *Stau1*, which is expressed ubiquitously, and *Stau2*, which is expressed predominantly in the brain (Buchner et al., 1999; Duchaine et al., 2002; Wickham et al., 1999). Functions of STAU2 relating to neuronal polarity, specifically dendritic spine formation and synaptic plasticity, have been described (Goetze et al., 2006; Lebeau et al., 2011; Ortiz et al., 2017; Popper et al., 2018), providing the impetus to gain a deeper understanding of the STAU2 RNA targets in mature brain (Maher-Laporte and DesGroseillers, 2010). In addition, the role of STAU2 in cortical development has been recognized. Studies of mid-gestation cortex development show that STAU2 is frequently expressed in dividing RGCs and is preferentially directed into the TBR2 (EOMES)<sup>+</sup> IPC daughter cell of an asymmetric RGC-IPC division (Kusek et al., 2012; Vessey et al., 2012). These observations raise the hypothesis that STAU2 may asymmetrically segregate RNA molecules that contribute to the IPC fate.

We and others have demonstrated that STAU2 binds thousands of different RNAs (Furic et al., 2007; Heraud-Farlow et al., 2013; Kusek et al., 2012), suggesting that STAU2 could influence the IPC fate by asymmetric delivery of a complex 'targetome' of RNAs. For example, the delivered RNA cargo could participate in suppression of RGC programs and stimulation of temporally appropriate IPC programs of gene expression, thus contributing to the dramatic differences in cell morphology, localization and division modes reflecting the RGC versus IPC fates. Moreover, we might expect that the cargo would change over time during corticogenesis, for example by distributing transcripts into IPCs that regulate the orderly production of specific types of neuronal or glial progeny.

<sup>1</sup>Neural Stem Cell Institute, Regenerative Research Foundation, Rensselaer, NY 12144, USA. <sup>2</sup>Nanobioscience Constellation, College of Nanoscale Science and Engineering, SUNY Polytechnic Institute, Albany, NY 12203, USA. <sup>3</sup>Department of Biochemistry and Molecular Biology, College of Medicine and Health Sciences, United Arab Emirates University, P.O. Box 17666, Al Ain, United Arab Emirates. \*These authors contributed equally to this work

<sup>†</sup>Author for correspondence (sallytemple@neuralsci.org)

DOI: 10.1242/dev.199376; S.A.A., 0000-0002-0483-4235; N.C.B., 0000-0002-9253-9411; S.T., 0000-0001-7301-783X

Handling Editor: Paola Arlotta

Received 20 December 2020; Accepted 5 July 2021

To identify transcriptome-wide RBP-binding events, techniques such as RNA-binding protein immunoprecipitation (RIP) followed by microarray (RIP-chip) (Tenenbaum et al., 2002), RIP followed by RNA sequencing (RIP-seq) (Zhao et al., 2010), and RNA crosslinking-immunoprecipitation (CLIP) and CLIP-seq have been developed (Licatalosi et al., 2008; Ule et al., 2003; Yeo et al., 2009). RIP-seq and CLIP-seq have been utilized to identify the typically thousands of diverse RNA targets of RBPs involved in neural development and function, such as TDP43 (TARDBP) (Sephton et al., 2011), AGO2 (Malmevik et al., 2015), HuR (ELAVL1) (Lebedeva et al., 2011), FMRP (FMR1) (Maurin et al., 2018) and others. However, none has examined how the cargo changes over time to provide an understanding of how stable or dynamic it may be.

Here, we perform RIP-seq at four major time points during mouse corticogenesis to capture early and late periods of neurogenesis and gliogenesis. We show that STAU2 binds a set of 3724 ‘stable’ genes important for RNA and protein metabolism, cell cycle processes, protein localization and other housekeeping-related activities at all ages examined. In addition, we identify a subset of 4244 genes in the cargo that are enriched at specific periods of corticogenesis; these ‘dynamic’ genes include transcription factors known to specify cortical progenitor and neuron subtype production. These data support the concept that STAU2, by binding and asymmetrically localizing a large number of RNAs, contributes to production of two very different progenitor cell types (an RGC and an IPC) in a single asymmetric division, and further that dynamic changes in the cargo can help to ensure that the type of IPC generated is altered over time to achieve the ordered temporal production of cells during corticogenesis.

## RESULTS

### STAU2 is expressed throughout embryonic corticogenesis in germinal and differentiating zones

We previously demonstrated a role for STAU2 in regulating asymmetric divisions during mouse cortical neurogenesis concentrating on a single mid-gestation time point, embryonic day (E) 15 (Kusek et al., 2012). Here, we studied STAU2 function throughout corticogenesis. We first examined its expression at four time points (Fig. 1), reflecting radial glia expansion and onset of neurogenesis (E11.5), deep layer (DL) formation (E13.5), upper layer (UL) formation (E15.5), and transition to gliogenesis (E17.5) (Cadwell et al., 2019). Cells were co-immunostained for TBR2, which labels IPCs (Englund et al., 2005), and  $\beta$ III-tubulin (BTUB), an early neuronal marker (Easter et al., 1993; Moody et al., 1989). At E11.5, TBR2<sup>+</sup> and BTUB<sup>+</sup> cells were observed in the preplate (PP) and STAU2 was expressed throughout the neuroepithelium with higher expression near the ventricular surface and in the PP (Fig. 1A). At E13.5, TBR2<sup>+</sup> cells were seen in the emerging SVZ, BTUB<sup>+</sup> neurons in the emerging cortical plate (CP) and STAU2 immunostaining was found throughout the layers (Fig. 1B). At E15.5 and E17.5, when mainly the deep and upper cortical layers are being produced, respectively (Fig. 1C,D), STAU2 expression was still robust in the remaining germinal VZ and SVZ layers and was present in the CP, fitting its known role in dendritogenesis.

To examine cell type-specific STAU2 expression, we co-immunostained for PAX6, a marker of RGCs (Götz et al., 1998), and phosphohistone H3 (PHH3) to identify mitotic cells (Hendzel et al., 1997). At E13.5 and E15.5, STAU2 was expressed in PAX6<sup>+</sup> cells in the VZ, and in PHH3<sup>+</sup> mitotic cells (Fig. 1E-H). Interestingly, at E17.5, when the cortical layers are becoming stratified (Britanova et al., 2008), STAU2 was most highly

expressed in layer V BCL11B (also known as CTIP2)<sup>+</sup> cells (Fig. S1A). Collectively, these results show that STAU2 is expressed in PAX6<sup>+</sup> RGCs, TBR2<sup>+</sup> IPCs and differentiating cortical neurons throughout corticogenesis, with particularly robust expression in layer V cells at E17.5.

### RIP-seq defines global STAU2 cargo at different stages of corticogenesis

We used an anti-STAU2 antibody to pull down bound RNA molecules (Jayaseelan et al., 2011) at these four stages of corticogenesis (E11.5, E13.5, E15.5 and E17.5), performing three independent experimental replicates. Briefly, cortical tissue was lysed, incubated with anti-STAU2-coated Protein A/G beads, and, after washing, the bound RNA was extracted. A portion of the starting material (cortical cell lysate) was used as input control that was not subjected to RIP. RNA sequencing was performed on the STAU2 RIP and input samples. To identify the STAU2 targetome, we utilized a peak-calling algorithm that provides high sensitivity to detect enrichment of STAU2-bound transcripts, followed by a Bayesian approach to determine differential binding over the time course (Fig. 2A).

After the RNA-seq count data were mapped to the UCSC mm10 reference genome, HOMER (Heinz et al., 2010) was used to identify peaks statistically enriched at least 4-fold over input and commonly across all three replicates. Regions of high sequencing read density that mapped to a specific location on either strand were considered peaks, and those significantly enriched in the STAU2 RIP over input were considered STAU2 cargo. Peaks thus obtained were further stratified based on peak score given by HOMER (Fig. S2A). Of a total of 35,034 peaks, 12,763 had a peak score of less than ten, 18,795 had peak scores between ten and 100, and 3476 had peak scores higher than 100 (Fig. S2A). To select for transcripts most enriched in the cargo, we assessed the peak trajectory (Fig. S2B) and used the point of maximum curvature (the elbow of the curve) as a cut-off, corresponding to a peak score of 12.5. By removing peaks in the more incremental regime (below the cut-off) we sought to reduce the likelihood of including false positives in our analysis. As the scores increase more rapidly after the cut-off, we expect them to reflect meaningful features of our system more accurately. Peaks with scores greater than 12.5 (18,975) corresponded to 7968 genes, which were analyzed further (Table S1). We then validated candidate RNAs by RIP combined with quantitative real-time PCR (qRT-PCR) and found significant enrichment in STAU2 pulldowns versus IgG controls (Fig. S2C). Given that *Stau2* expression is low in developing brain and spinal cord endothelial cells (Rosenberg et al., 2018; Zeisel et al., 2015; Zhang et al., 2014), we also assessed endothelial cell transcript binding as a measure of potential post-lysis, non-specific transcript binding, and found this to be extremely low (see Supplementary Materials and Methods), as expected given our protocol was optimized to reduce this factor (Tenenbaum et al., 2002; Penalva et al., 2004; Nicholson et al., 2017).

Distribution of the types of peaks identified and the genomic features associated with the peaks were analyzed using R. The majority of captured sequences were categorized as 3'UTR (6750), followed by exons (5983), intergenic (4513), 5'UTRs (1140) and introns (589) (Fig. 2B). A single peak was identified for 4508 genes, two or three peaks for 2797 genes and four or more for the remainder (661), with a maximum of 14 peaks per gene (Fig. 2C). As an example, we examined three genes belonging to the TATA-box-binding-protein-associated factor (TAF) family enriched in the cargo, *Taf10*, *Taf11* and *Taf13*, and found different patterns.

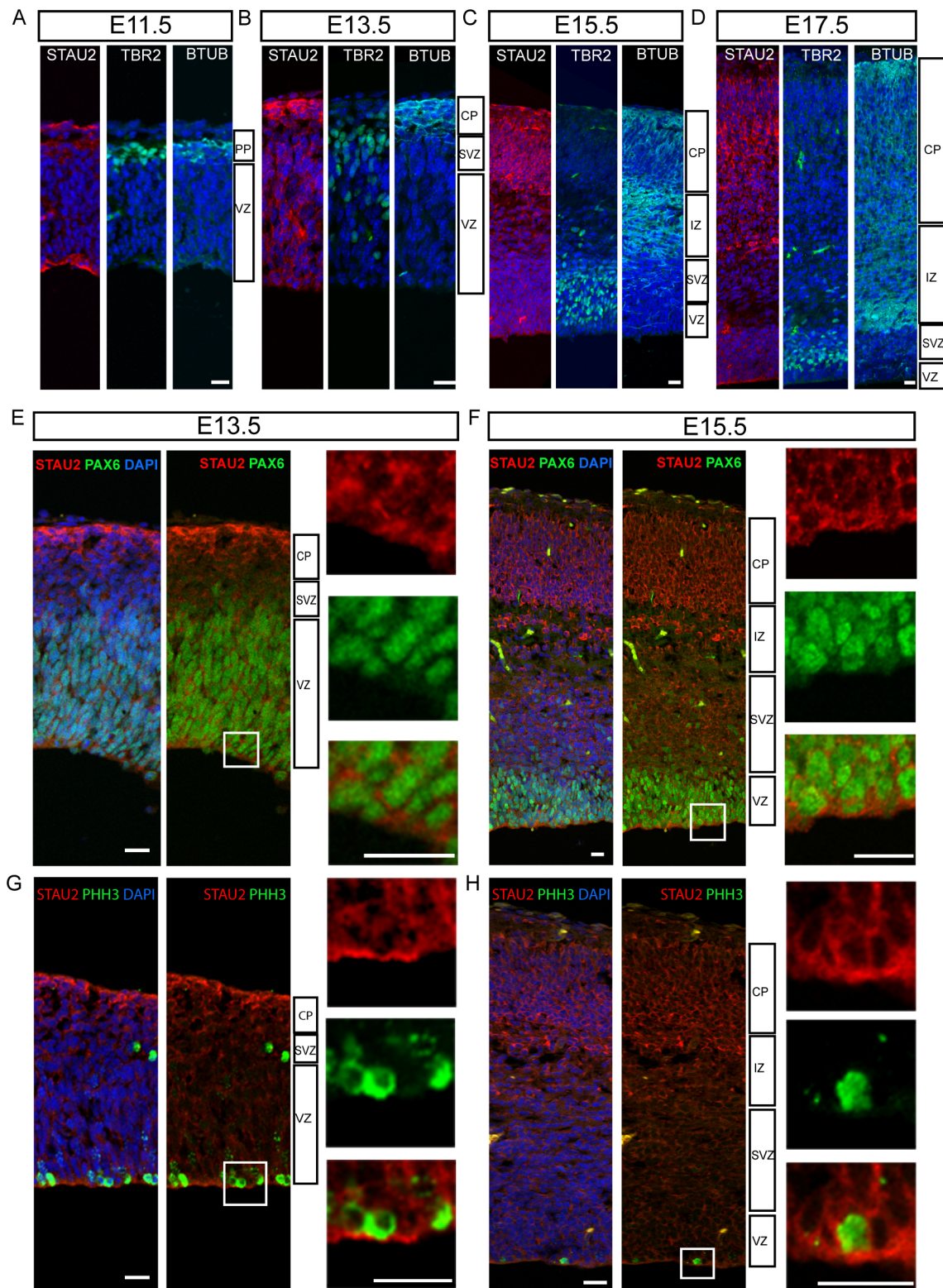


**Fig. 1. STAU2 is expressed throughout embryonic corticogenesis in germinal and differentiating zones.** (A–D) Immunohistochemistry using a STAU2-specific mouse monoclonal antibody in coronal sections reveals expression of STAU2 in the cortex at E11.5, E13.5, E15.5 and E17.5. TBR2 expression is observed in the PP at E11.5 and in the SVZ and VZ from E13.5 onwards. BTUB is expressed in the PP at E11.5, CP at E13.5, and CP and IZ at E15.5 and E17.5. (E–H) STAU2 is expressed in PAX6<sup>+</sup> cells (E,F) and in PHH3<sup>+</sup> cells (G,H) in the VZ at E13.5 and E15.5. Boxed areas are shown at higher magnification to the right as single and merged images. Scale bars: 20 μm. See also Fig. S1.

*Taf10* and *Taf13* transcripts each had peaks at two sites within exonic and 3'UTR regions, whereas *Taf11* peaks were observed in the 5'UTR and 3'UTR regions (Fig. S2D). Note that the location of

a peak was not used to identify its binding location, rather we interpret a peak as indicative of the presence of the transcript in the cargo.

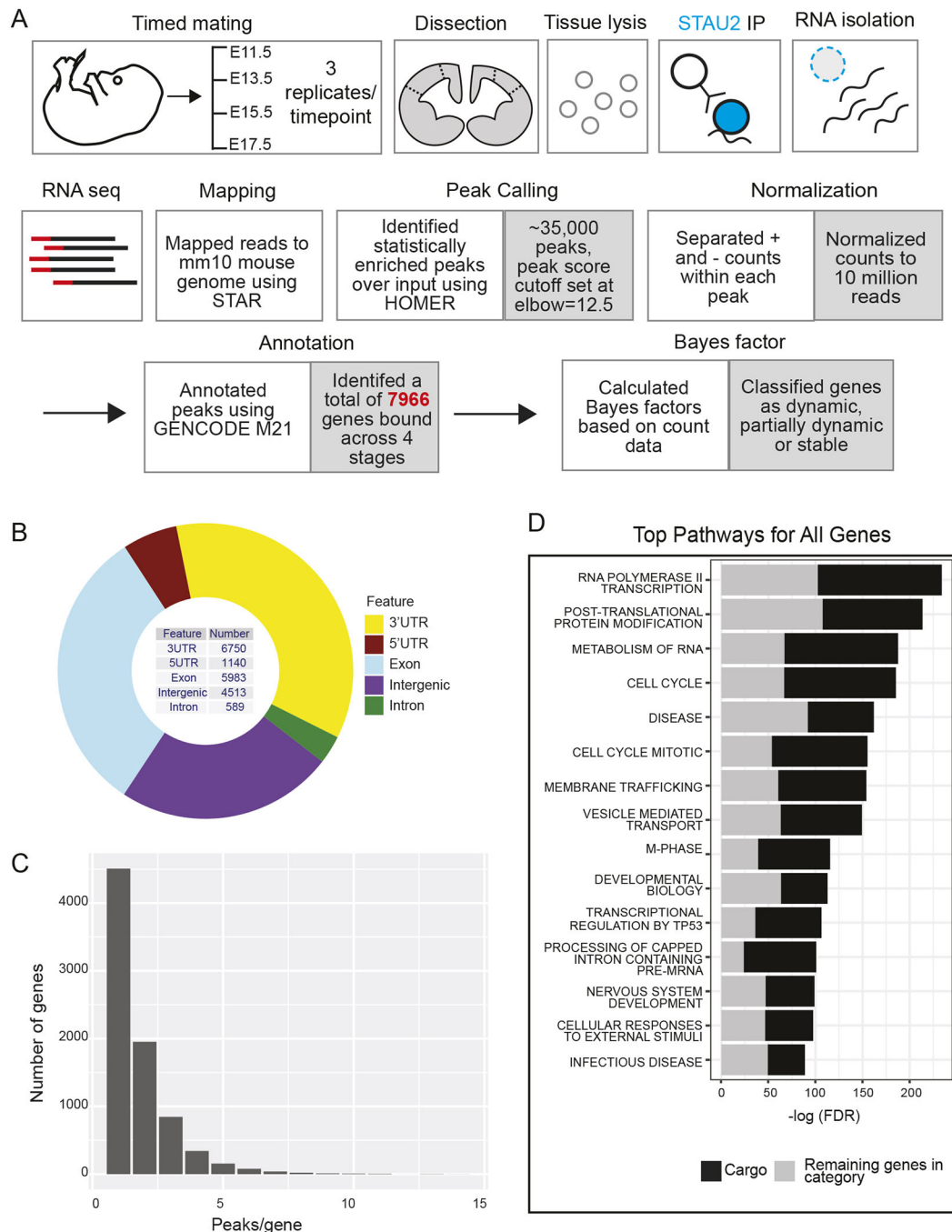


**Fig. 2. RIP-seq defines global STAU2 cargo at different stages of corticogenesis.** (A) Schematic depicting RIP-seq workflow. (B) Donut chart depicting the number of captured sequences corresponding to different genomic features. (C) Bar chart showing the distribution of number of peaks per gene in the cargo. (D) Top 15 REACTOME pathways for all STAU2-bound transcripts. To illustrate the contribution of STAU2 cargo to each category, the bars are filled to show the proportion of STAU2 cargo (black) versus the remaining genes in the category (gray). See also Fig. S2.

Having identified the STAU2 cargo across the span of corticogenesis at a global level, we used Reactome and Gene Ontology (GO) to identify cellular pathways (Fig. 2D, Table S3) and biological process (BP) categories (Fig. S2E, Table S3). Major pathways identified for all genes included ‘RNA polymerase II transcription’, ‘post-translational protein modification’, ‘metabolism of RNA, cell cycle’, ‘membrane trafficking’ and ‘vesicle-mediated transport’ (Fig. 2D). The top biological processes for all genes included several categories related to cell cycle and its regulation, ‘intracellular transport’ and ‘RNA processing’ (Fig. S2E). These

results demonstrate the diverse types of RNA in the STAU2 cargo and their contribution to a variety of processes.

#### A subset of STAU2 target transcripts is temporally regulated

Given our hypothesis that the STAU2 targetome changes during cortical development, we investigated whether a subset of the cargo was preferably bound at different time points, i.e. was dynamic in nature. A Bayesian approach was used to test whether transcripts were differentially bound across time (Jeffreys, 1998). Using R, a Bayes factor (BF) was assigned to each gene representing the degree

of differential binding between two consecutive time points, and  $\ln(\text{BF})$ s were summed across the time course (Table S2). A higher BF corresponded to greater evidence for variability in binding above input across time whereas a lower score signified greater consistency. This analysis discriminated changes at the level of STAU2 binding of a particular target from changes occurring in the expression level (input) of that target. We assigned RNA targets in the cargo to distinct groups based on the evidence categories

outlined by Jeffreys (1998) (Fig. 3A): 12% were strongly variable in their interaction with STAU2 over time ('dynamic'), 41% were moderately variable ('partially dynamic') and 47% showed no significant difference in binding and were considered 'stable' (Fig. 3B).

To identify enriched categories for biological processes and cellular pathways, we applied the HypeR enrichment function in R using genesets available from GO and Reactome (Fig. 3C,D,

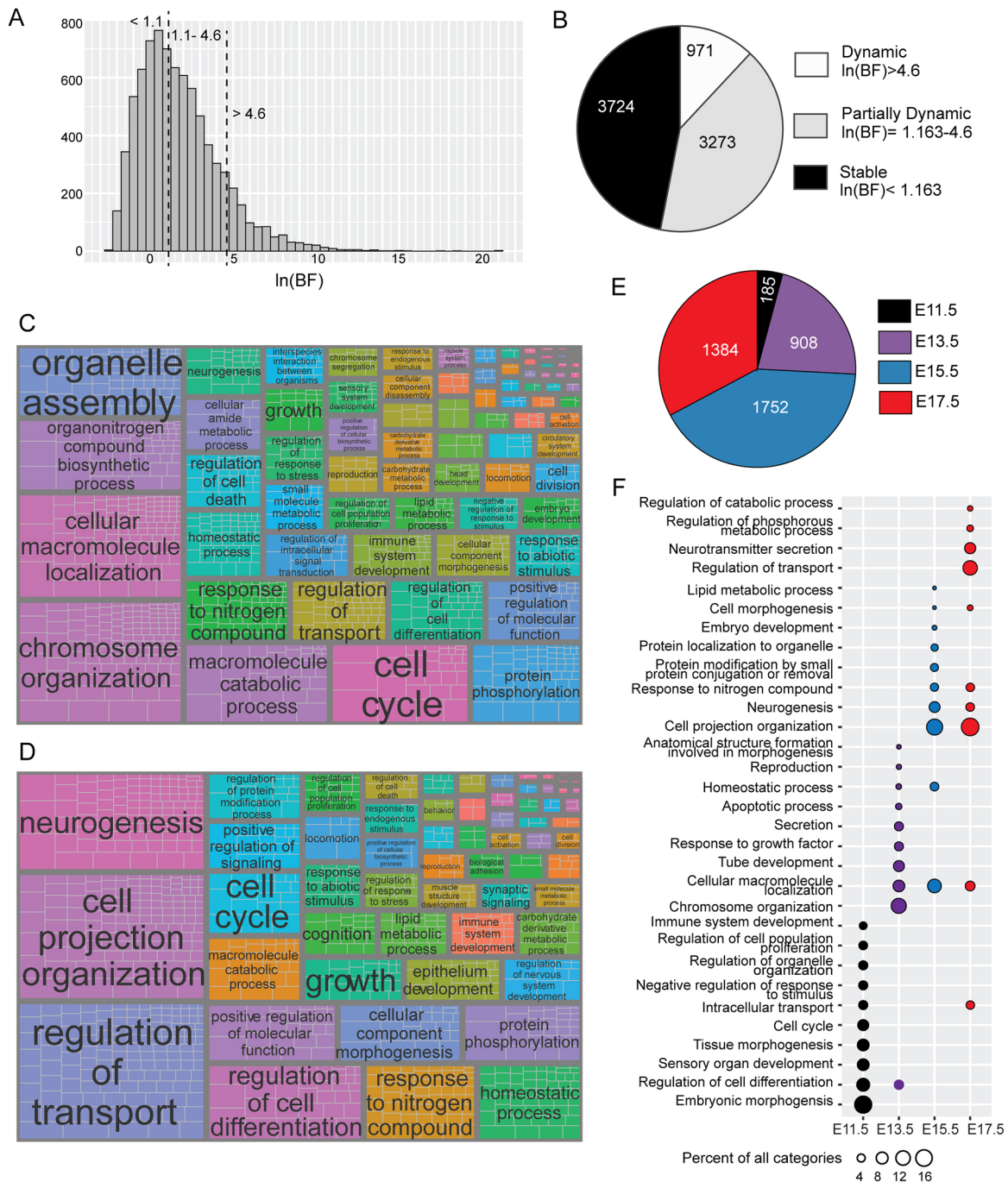


**Fig. 3. A subset of STAU2 target transcripts is temporally regulated.** (A) Bar chart showing the distribution of number of genes in STAU2 cargo as a function of summed  $\ln(\text{BF})$  [denoted here as  $\ln(\text{BF})$ ]. (B) Pie chart showing the classification of STAU2-bound transcripts as dynamic, partially dynamic, or stable. (C,D) TreeMaps showing GO biological process (BP) categories associated with stable (C) and dynamic (D) transcripts in the STAU2 cargo. (E) Pie chart showing the number of transcripts most highly bound by STAU2 at E11.5, E13.5, E15.5 and E17.5. Dynamic and partially dynamic genes were used for this analysis (14 genes had the same maximal read counts at two time points and were not included in the figure). (F) Balloon graph showing the top parent Reactome pathways associated with the most highly bound transcripts at each time point. See also Fig. S3.

Tables 1 and 2, Tables S4-S6). The top GO biological process categories for the stable group included ‘chromosome organization’, ‘cellular macromolecule localization’, ‘organonitrogen compound biosynthetic process’ and ‘organelle assembly’ (Fig. 3C). Stable transcripts were thus associated with activities related to general cellular maintenance. In contrast, the top biological process and pathways for the ‘dynamic’ genes included ‘neurogenesis’, ‘cell projection organization’, ‘regulation of transport’ and ‘regulation of cell differentiation’ (Fig. 3D).

To gain further insight into the mechanistic differences between pathways for stable and dynamic genes, we consolidated all pathways for each group into the top (parent) and second tier pathways in the Reactome pathway hierarchy (Fig. S3) and compared these. We noted that the ‘extracellular matrix (ECM) organization’ category was only enriched in the dynamic group and included pathways related to proteoglycans, syndecan interactions, collagen formation, assembly and degradation, and integrin cell-surface interactions. ‘Neuronal system’, a category associated with chemical transmission across synapses, activation of NMDA receptors and post-synaptic events, and pre-synaptic depolarization and calcium channel opening, was more enriched in the dynamic gene set. Other parent categories higher in the dynamic group included ‘vesicle-mediated transport’ with downstream pathways such as Golgi-ER retrograde and anterograde transport, membrane trafficking, and gap junction trafficking and regulation (Table S7). ‘Transport of small molecules’, including ion channel transport, was most highly enriched in the partially dynamic category. Pathways such as ‘signaling by TGF $\beta$  family members’, ‘programmed cell death’, ‘DNA replication, cell cycle checkpoints’, ‘MAPK family signaling cascades’ and ‘metabolism of lipids’ were associated with partially dynamic and stable groups. ‘Protein localization’, ‘chromatin organization’, ‘cell-cell communication’ and ‘chromosome maintenance’ parent pathways were higher in the stable group. Others, such as ‘nervous system development’, ‘metabolism of RNA’, ‘DNA repair’, ‘signaling by receptor tyrosine kinases’, ‘RNA polymerase II transcription’, ‘metabolism of proteins’, ‘cell cycle’ and ‘immune system’, were enriched across the entire cargo.

We then examined biological processes associated with genes most highly bound at each time point (Fig. 3E, Table S8). At E11.5,

‘embryonic and tissue morphogenesis’, ‘regulation of cell proliferation’ and ‘cell differentiation’ were among the most enriched processes. At E13.5 and E15.5, GO categories such as ‘chromosome organization’ and ‘macromolecule localization’ were highly represented. GO terms associated with ‘neurogenesis’ and ‘cell projection organization’ were highest at E15.5 and E17.5 whereas ‘neurotransmitter secretion’ and ‘regulation of transport’ were most enriched at E17.5 (Fig. 3F). Together, these analyses suggest that STAU2 participates in fundamental cell processes across corticogenesis and also developmentally regulated processes by altering subsets of genes bound at different time points.

### STAU2 binds pro- and non-IPC genes in a developmental stage-dependent manner

To validate the stable and dynamic nature of the cargo, we chose three of the top biological process and pathway categories associated with the dynamic and stable STAU2 cargo genes (Tables 1 and 2), selected five or six genes from each category, and plotted their level of expression over time (Fig. 4A). This confirmed the stable versus dynamic expression, and revealed how dynamic genes in the cargo changed, with some building steadily over the time course, such as *Map6* and *Acap3*, and others peaking at mid-gestation, such as *Auts2* and *Cdon*. To further validate our approach, we confirmed the presence of several dynamic and stable transcripts in STAU2 cargo at E15.5 and E17.5 by performing qRT-PCR on RNA isolated from independent STAU2 RIPs (Fig. S4). Given the role of IPCs in cortical neuron production (Mihalas et al., 2016), we then asked whether the STAU2 RNA targetome included IPC determinants.

To explore the role of STAU2 in IPC specification, we compared the STAU2 cargo with previously published datasets of genes with defined roles in IPC formation and neuronal differentiation. Transcriptome data from FACS-isolated proliferating progenitors (defined as symmetrically expanding progenitor cells, mostly RGCs in the VZ), differentiating progenitors, and neurons in E14.5 mouse cortex were used to identify candidate genes functionally important in IPC specification (Aprea et al., 2013). Genes enriched in IPCs versus proliferating progenitors and neurons (ON-switch genes in Aprea et al., 2013) and those enriched in proliferating progenitors and neurons over IPCs (OFF-switch genes) are termed ‘pro-IPC’ genes and ‘non-IPC’ genes here, respectively. The STAU2 cargo

**Table 1. Top 20 Reactome pathways enriched in stable STAU2 cargo**

Category name	P-value	FDR	Gene set	Overlap
REACTOME_RNA_POLYMERASE_II_TRANSCRIPTION	4.20E-104	6.50E-101	1112	305
REACTOME_METABOLISM_OF_RNA	1.30E-92	9.90E-90	657	219
REACTOME_POST_TRANSLATIONAL_PROTEIN_MODIFICATION	1.60E-81	8.30E-79	1370	308
REACTOME_CELL_CYCLE	2.20E-75	8.40E-73	655	198
REACTOME_DISEASE	1.40E-70	4.50E-68	1481	304
REACTOME_TRANSCRIPTIONAL_REGULATION_BY_TP53	7.70E-65	2.00E-62	353	134
REACTOME_CELL_CYCLE_MITOTIC	7.10E-58	1.60E-55	523	155
REACTOME_INFECTIOUS_DISEASE	1.80E-48	3.50E-46	776	178
REACTOME_CELLULAR_RESPONSES_TO_EXTERNAL_STIMULI	4.00E-48	6.90E-46	563	148
REACTOME_MEMBRANE_TRAFFICKING	1.20E-43	1.80E-41	616	149
REACTOME_PROCESSING_OF_CAPPED_INTRON_CONTAINING_PRE_MRNA	1.90E-43	2.70E-41	240	90
REACTOME_M_PHASE	9.30E-42	1.20E-39	381	112
REACTOME_DNA_REPAIR	2.30E-41	2.80E-39	310	100
REACTOME_VESICLE_MEDIATED_TRANSPORT	4.00E-40	4.40E-38	672	151
REACTOME_MRNA_SPLICING	1.20E-37	1.20E-35	188	74
REACTOME_HIV_INFECTION	5.60E-37	5.40E-35	224	80
REACTOME_CHROMATIN_MODIFYING_ENZYMES	6.50E-37	6.00E-35	247	84
REACTOME_TRANSLATION	2.10E-34	1.80E-32	289	88
REACTOME_REGULATION_OF_TP53_ACTIVITY	1.20E-33	9.80E-32	158	64
REACTOME_DEVELOPMENTAL_BIOLOGY	6.00E-32	4.70E-30	1011	177

Table 2. Top 20 Reactome pathways enriched in dynamic STAU2 cargo

Category name	P-value	FDR	Gene set	Overlap
REACTOME_RNA_POLYMERASE_II_TRANSCRIPTION	6.10E-32	9.40E-29	1112	88
REACTOME_DEVELOPMENTAL_BIOLOGY	2.20E-28	1.70E-25	1011	79
REACTOME_NEURONAL_SYSTEM	1.20E-25	6.20E-23	398	48
REACTOME_VESICLE_MEDIATED_TRANSPORT	1.60E-25	6.30E-23	672	61
REACTOME_NERVOUS_SYSTEM_DEVELOPMENT	1.10E-23	3.30E-21	567	54
REACTOME_MEMBRANE_TRAFFICKING	1.50E-23	3.90E-21	616	56
REACTOME_POST_TRANSLATIONAL_PROTEIN_MODIFICATION	7.20E-22	1.60E-19	1370	82
REACTOME_TRANSMISSION_ACROSS_CHEMICAL_SYNAPSES	1.20E-20	2.40E-18	260	35
REACTOME_SIGNALING_BY_RHO_GTPASES	2.30E-16	3.90E-14	419	38
REACTOME_DISEASE	4.20E-16	6.50E-14	1481	75
REACTOME_DOPAMINE_NEUROTRANSMITTER_RELEASE_CYCLE	5.00E-14	7.00E-12	23	11
REACTOME_SEROTONIN_NEUROTRANSMITTER_RELEASE_CYCLE	9.90E-14	1.30E-11	18	10
REACTOME_SIGNALING_BY_RECEPTOR_TYROSINE_KINASES	3.30E-13	4.00E-11	501	37
REACTOME_METABOLISM_OF_RNA	4.10E-12	4.60E-10	657	41
REACTOME_CYTOKINE_SIGNALING_IN_IMMUNE_SYSTEM	4.60E-12	4.70E-10	837	47
REACTOME_ADAPTIVE_IMMUNE_SYSTEM	2.00E-11	2.00E-09	721	42
REACTOME_NEUROTRANSMITTER_RECEPTORS_AND_POSTSYNAPTIC_SIGNAL_TRANSMISSION	5.10E-11	4.70E-09	196	21
REACTOME_METABOLISM_OF_CARBOHYDRATES	5.70E-11	4.90E-09	284	25
REACTOME_NCAM_SIGNALING_FOR_NEURITE_OUT_GROWTH	6.20E-11	5.10E-09	63	13
REACTOME_NEUROTRANSMITTER_RELEASE_CYCLE	6.50E-11	5.10E-09	51	12

profile included 73 of the 208 pro-IPC (35%) genes and 78 of the 207 (37.6%) non-IPC genes. Of these, approximately two-thirds of the genes in each group were dynamic in their interaction with STAU2 (Fig. 4B, Table S9) and these were visualized across time using the heatmap function in R (Fig. 4C,D). Interestingly, pro-IPC genes were elevated in the cargo at E13.5 and E15.5 in comparison with E11.5 and E17.5 (Fig. 4C), corresponding to IPC production at mid-gestation. Non-IPC genes were highest at E17.5 and bound less frequently at E11.5 and E13.5 (Fig. 4D). This, combined with the knowledge that STAU2 is asymmetrically distributed into TBR2<sup>+</sup> IPCs (Kusek et al., 2012), is consistent with the model in which STAU2 carries a set of IPC determinants during mid-corticogenesis that are then unbound at a later stage coinciding with the termination of neurogenic IPC production.

**STAU2 cargo includes cortical determinants associated with nervous system phenotypes**

To understand whether STAU2 carries transcripts that help determine cell identity during IPC subtype specification, we first identified which targets in the cargo were enriched in mouse cortical germinal zones using transcriptomes obtained at mid-gestation (Fietz et al., 2012). A substantial proportion (45-50%) of genes they identified as markers of the VZ and SVZ are present in the STAU2 cargo (Fig. S5A). Understanding the key role that transcription factors and chromatin modifiers play in progenitor cell and progeny specification, we then filtered these gene sets to obtain the DNA-binding (DB) genes specific for each germinal zone (Fig. S5A, Table S10).

Given that most IPCs are located in the SVZ, we first identified DB genes expressed in the SVZ by combining those unique to the SVZ with those common to the SVZ and VZ, denoted as ‘SVZ-DB’. SVZ-DB genes were highly enriched in the cargo at E13.5 and E15.5 (Fig. 5A). A significant proportion of the SVZ-DB genes peaked at the mid-stages of neurogenesis with almost no presence at E11.5 and E17.5 (upper panel). Genes highest at E13.5 included *Emx1*, important for production of cortical excitatory neurons and glia (Gorski et al., 2002), *Cux1*, an UL marker involved in dendritic branching, spine and synapse formation in later-born layer II/III cells (Cubelos et al., 2010), and *Cdk12*, associated with neurogenesis and microcephaly (Chen et al., 2017a). Genes with

highest expression at E15.5 included the neuron-promoting IPC determinants, *Myt1*, *Neurod1* (Kawaguchi et al., 2008) and *Scrt2* (Paul et al., 2014). Another large group (lower panel) was present from E13.5 to E17.5 but with maximal binding at E15.5, and included regulators of neurogenesis timing, such as *Hes6* and *Hbp1*. *Hes6*, an IPC marker (Kawaguchi et al., 2008) was found to inhibit astrocyte formation and promote neuronal differentiation (Jhas et al., 2006), whereas deficiency of *Hbp1* delayed neuronal differentiation and disrupted cortical morphogenesis via altered cell cycle progression (Watanabe et al., 2015). This group also included genes prominent at E17.5 that are associated with layers II/III, such as *Cited2*, *Pou3f3*, *Satb2*, *Hivep3* (Belgard et al., 2011; Fame et al., 2016; Sugitani et al., 2002; Tasic et al., 2018), astrocytes, such as *Srehfl* (Loo et al., 2019), and interneurons, e.g. *Dlx2* (Petryniak et al., 2007), and therefore may be involved in the transition of progenitor cells into later-born cell types.

We then performed a similar assessment of cortical plate DNA-binding (CP-DB) genes (Fig. S5B). Predictably, most were enriched in the cargo at E17.5 and these included genes associated with neurodevelopmental disorders in humans, such as *Deaf1* (Chen et al., 2017b), intellectual disability, such as *Grin1* (Lemke et al., 2016), and schizophrenia, such as *Nr4a3* (Novak et al., 2010) and *Ppp1r1b* (Wang et al., 2017). Other CP-DB genes in the E17.5 group included *Crtcl*, involved in dendritic growth of cortical neurons and linked to Alzheimer’s disease (Li et al., 2009; Parra-Damas et al., 2014), and *Nfix*, important for astrocytic gene expression during CNS development (Gopalan et al., 2006; Matuzelski et al., 2017) and oligodendrogenesis in the forebrain (Zhou et al., 2015). Moreover, CP-DB genes enriched at mid-stages of corticogenesis included *Cdh13*, *Fezf2*, and other genes belonging to the Nfi family, *Nfia* and *Nfib*, known to be essential for mouse forebrain development.

*Fezf2* (present in the cargo at all stages, and highly bound at E13.5 and E15.5) is necessary and sufficient for production of DL subcerebral projection neurons (Chen et al., 2005; Molyneaux et al., 2005). *Cdh13*, an attention deficit hyperactivity disorder (ADHD)-associated gene, is involved in brain network formation (Rivero et al., 2013) and its loss late in development caused a decrease in interneurons and late-born pyramidal neurons with increased cell death (Killen et al., 2017). *Nfib* is highly expressed both in RGCs and corticofugal projection neurons, and knockout mice show

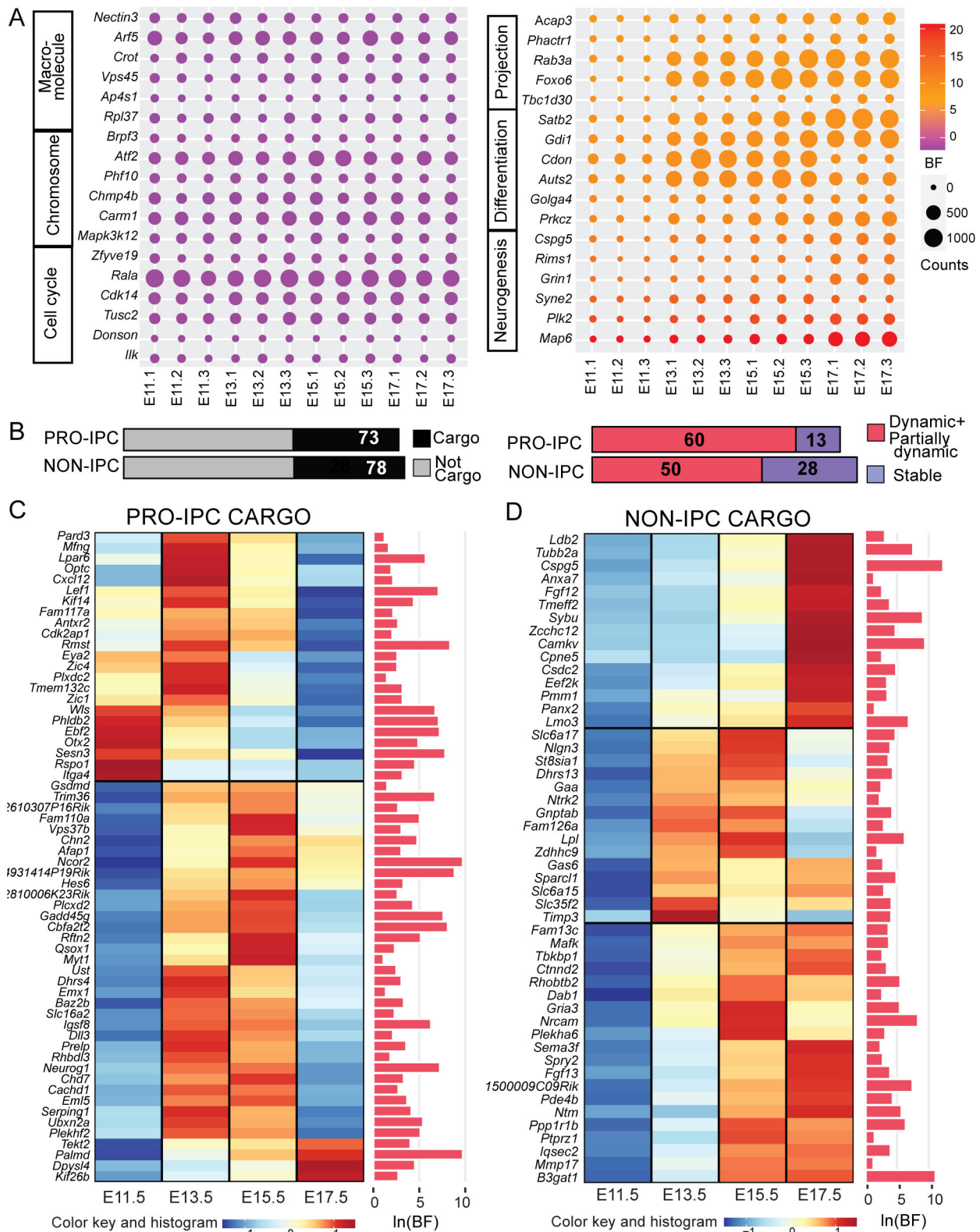


**Fig. 4. STAU2 binds pro- and non-IPC genes in a developmental stage-dependent manner.** (A) Dot plot showing the expression of representative transcripts related to top GO biological processes for stable genes (left; macromolecule localization, chromosome organization, and cell cycle) and top GO biological processes for dynamic genes (right; neurogenesis, differentiation, and cell projection organization) across three replicates for the four time points. Counts represent the magnitude of expression and the Bayes factor (BF) reflects variability across time, with purple and red signifying low and high BFs, respectively. (B) Bar graph showing the proportion of pro-IPC and non-IPC genes identified by Aprea et al. (2013) in the STAU2 cargo (left), and proportions of dynamic and stable pro-IPC and non-IPC cargo genes (right). (C,D) Heatmaps showing the expression of dynamic and partially dynamic pro-IPC genes (C) and non-IPC genes (D) in the STAU2 cargo from E11.5 to E17.5 (three replicates at each time point). Horizontal bar graphs next to each heatmap represent  $\ln(\text{BF})$ . Color key represents z-score after scaling across rows, with red and blue signifying higher and lower expression, respectively. See also Fig. S4.

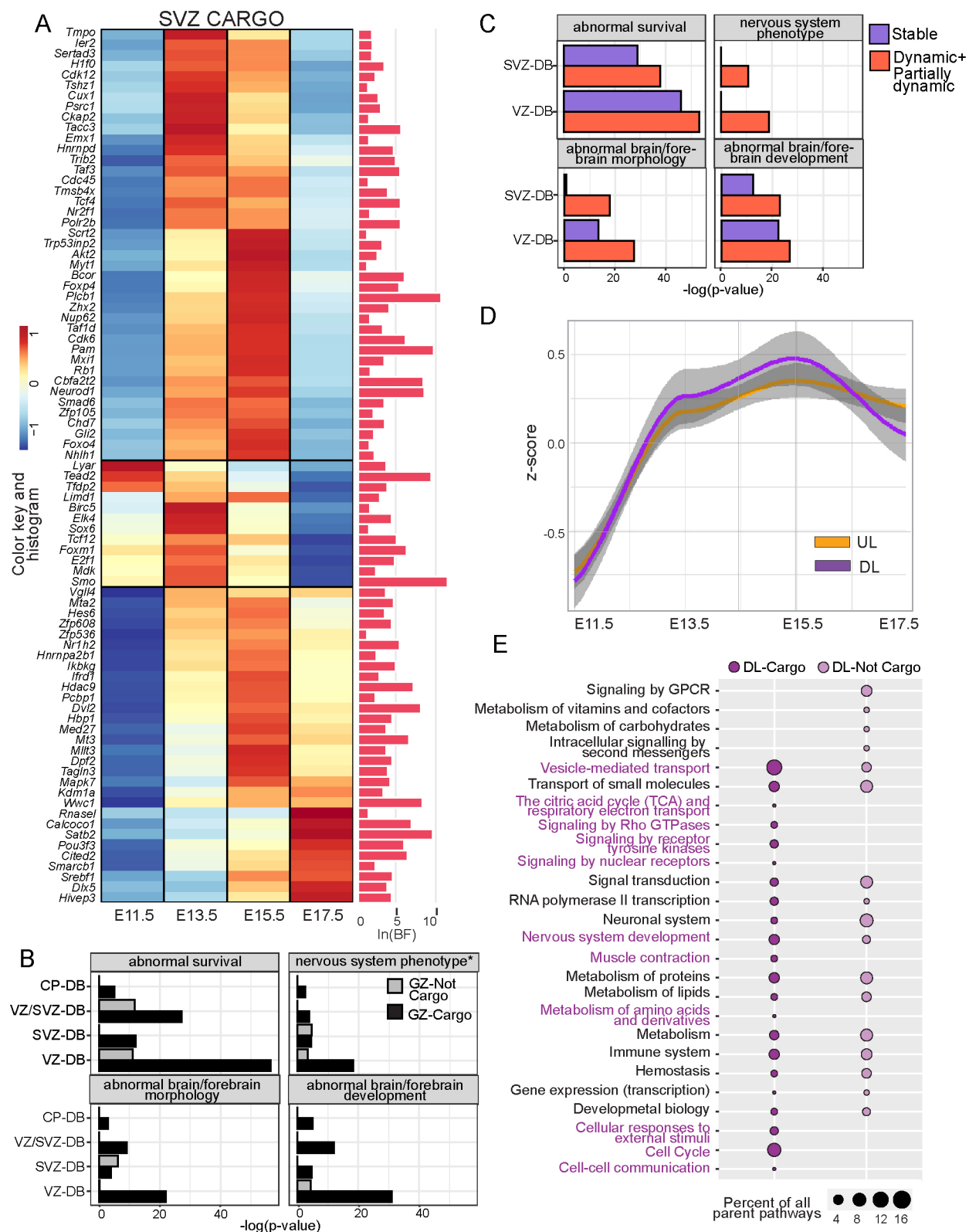


Fig. 5. See next page for legend.

defects in UL neuronal migration, DL axon projection and a reduction in outer RGCs and IPCs (Betancourt et al., 2014). *Nfia* also plays a crucial role in astrocyte formation with *Sox9* (also present in STAU2 cargo with highest binding at mid-neurogenesis) (Kang et al., 2012). These results show that STAU2 selectively

binds SVZ and CP DB genes, including key determinants of cortical cell subtypes, at appropriate stages of corticogenesis.

We then investigated whether DB genes in the cargo are more important for normal brain development than those not present in the cargo by performing a phenotypic enrichment. STAU2 cargo

**Fig. 5. STAU2 cargo includes cortical determinants associated with nervous system phenotypes and layer markers.** (A) Heatmap showing the average expression of dynamic and partially dynamic SVZ-DB genes in the STAU2 cargo from E11.5 to E17.5. The horizontal bar graph next to the heatmap represents  $\ln(\text{BF})$ . Color key represents z-score after scaling across rows, with red signifying higher expression and blue signifying lower expression. (B) Bar graphs depicting the phenotypic enrichment of STAU2-bound (GZ-Cargo) and not bound (GZ-Not Cargo) CP-DB, VZ/SVZ-DB, SVZ-DB and VZ-DB genes identified by Fietz et al. (2012) using the MGI database and MouseMine portal to determine Mammalian Phenotype Ontology Enrichment. Note that for CP-DB, 'nervous system phenotype' was not enriched, therefore it was substituted with the *P*-value for a related category 'abnormal learning/memory/conditioning'. (C) Bar graphs depicting Mammalian Phenotype Ontology Enrichment of dynamic+partially dynamic and stable SVZ-DB and VZ-DB genes in the STAU2 cargo. (D) Line graph showing the cumulative expression of upper layer and deep layer markers from E11.5 to E17.5. The gray shading denotes the confidence interval (90%) for each time point. (E) Balloon plot showing enriched Reactome parent pathways, i.e. the top tier and the second tier pathways associated with DL genes. Dark and light purple indicates pathways associated with STAU2 cargo and 'not cargo' genes, respectively. Percentage is indicated by dot size and refers to the contribution of the specified category to all the enriched categories. See also Fig. S5.

DB genes are more strongly associated with developmental phenotypes such as survival (including lethality during fetal growth through weaning, perinatal lethality and postnatal lethality), brain/forebrain development, nervous system phenotypes and brain/forebrain morphology compared with 'not cargo' DB genes (Fig. 5B). Moreover, dynamic SVZ-DB genes were significantly more enriched for brain/forebrain and nervous system developmental phenotypes (Fig. 5C).

#### Cortical layer markers are present in the STAU2 cargo

Having established that STAU2 carries a subset of germinal zone DB transcripts that contribute to developmental phenotypes, we then asked whether the STAU2 RNA targetome included cortical layer markers that were temporally regulated. We utilized a previously published dataset to identify layer-enriched genes and then evaluated the mean expression of these markers in the cargo (Fig. 5D). Sequencing of microdissected adult mouse neocortical layer samples, together with RNA *in situ* hybridization, produced calibrated probabilities of genes enriched in cortical layers II-III, layer IV, layer V, layer VI and layer VIIb (Belgard et al., 2011). To generate lists of layer-specific markers, we first scaled these probability values across all layers using the empirical cumulative distribution function (ECDF) function in R, and then selected genes with scaled probability values  $>0.9$  as layer-specific markers. We thus categorized the genes in the Belgard et al. dataset as UL or DL markers. A total of 882 genes were exclusive to the UL and 1249 genes to the DL, and, of these, a significant proportion, 325 (37%) UL and 478 (38%) DL markers, were present in the STAU2 cargo. We analyzed the cumulative expression of STAU2-bound layer markers with weights based on the probability of being UL or DL, to calculate the weighted mean expression of UL and DL markers in the cargo at the four time points, shown with a 90% confidence interval (Fig. 5D). Although both DL and UL-associated genes in the cargo increased from E11.5 to E13.5, DL genes decreased after E15.5 whereas UL genes remained high. Hence, the STAU2 cargo includes key genes important for cortical neuron identity that change over time.

Next, we assessed enriched pathways for UL and DL genes, first consolidating pathways for STAU2 cargo and 'not cargo' genes into the top (parent) and second tier pathways in the Reactome pathway hierarchy (Fig. 5E, Fig. S5C,D, Table S11). Cell cycle categories, vesicle-mediated transport and signaling pathways were more

enriched in the cargo DL markers compared with those not in the cargo. Pathways specific for cargo UL genes included Eph-Ephrin signaling pathways and pathways related to synaptic cell adhesion molecules, neurexins and neuroligins (Fig. S5C). STAU2 has previously been linked to long-term potentiation (Berger et al., 2017), and alterations in synaptic plasticity and neurexins and neuroligins are implicated in autism and other cognitive conditions (Hansel, 2019; Südhof, 2008), connecting STAU2 cargo to UL-related cognitive disorders. Interestingly, although pathways related to the respiratory electron transport chain and TCA cycle were strongly associated with DL genes and the STAU2 targetome in general, they were not enriched in the UL cargo but were instead associated with non-cargo UL genes (Fig. S5C,D, Table S11). This observation indicates that STAU2 specifically binds transcripts related to such metabolic processes in the context of DL but not UL cells. Overall, these results make it clear that there is a distinct functional difference between transcripts bound and not bound by STAU2 that may contribute to appropriate specification and function of the cortical layers.

We found by immunostaining that STAU2 is most enriched in layer V cells at E17.5 and in adult mouse brain (Fig. S1B), and STAU2 has been characterized as a layer V marker in the adult brain (Belgard et al., 2011). To investigate this connection further, we performed pathway analysis of layer V genes in the STAU2 cargo and found significantly enriched pathways, such as membrane trafficking, vesicle-mediated transport, post-translational protein modification, and transport of small molecules (Table 3). The top categories also included cellular metabolism-linked pathways, such as TCA cycle and respiratory electron transport (Table 3, in bold). Hence, STAU2 binds transcripts involved in energy metabolism and ATP synthesis specifically in layer V cells, which may be particularly important for this layer (Agostini et al., 2016; Belgard et al., 2011).

#### Knockdown of a STAU2 target, *Taf13*, reduces OLIG2<sup>+</sup> cells

If STAU2 contributes to the appropriate distribution of fate determinants during asymmetric RGC/IPC divisions, we predict that altering cargo molecules, especially those associated with DB functions, will affect cortical development. One of the general transcription factors present in the cargo across developmental stages is TAF13. *Taf13* was significantly reduced after STAU2 knockdown (KD) in mouse embryonic cortical cultures *in vitro* (Fig. S6), corroborating findings made in rat cortical cultures (Heraud-Farlow et al., 2013). We then used shRNA lentiviral constructs to knock down *Taf13* in E13.5 cortical progenitor cells *in vitro*, achieving 80–90% lower expression (Fig. 6A). After 5 days *in vitro* (DIV), we examined neuronal and glial markers by qRT-PCR, and found a significant reduction in expression of *Olig2*, an oligodendrocyte lineage marker (Fig. 6B). *Mki67*, a mitotic cell marker, was slightly reduced after *Taf13* KD (Fig. 6C). The reduction of OLIG2<sup>+</sup> cells was confirmed by immunostaining (Fig. 6D,E). Although we observed a trend towards an increase in BTUB<sup>+</sup> neurons after *Taf13* KD, this was not statistically significant (Fig. 6F). These observations indicate that impaired STAU2 function could in turn reduce levels of *Taf13* and inhibit oligodendrogenesis. Hence, in addition to known IPC determinants, the STAU2 targetome is a resource for identifying previously unrecognized determinants of cortical cell fate during corticogenesis.

#### DISCUSSION

In this study, we investigated the nature and complexity of RNA molecules bound by STAU2 at four distinct stages of mouse corticogenesis. We found that although STAU2 binds a wide range of

**Table 3. Top 20 pathways enriched in layer V transcripts present in STAU2 cargo**

Category name	P-value	FDR	Gene set	Overlap
REACTOME_MEMBRANE_TRAFFICKING	1.50E-31	2.30E-28	616	63
REACTOME_VESICLE_MEDIATED_TRANSPORT	3.00E-30	2.30E-27	672	64
REACTOME_POST_TRANSLATIONAL_PROTEIN_MODIFICATION	6.00E-24	3.10E-21	1370	81
REACTOME_TRANSPORT_OF_SMALL_MOLECULES	8.60E-17	3.30E-14	713	48
REACTOME_ADAPTIVE_IMMUNE_SYSTEM	6.10E-16	1.90E-13	721	47
<b>REACTOME_THE_CITRIC_ACID_TCA_CYCLE_AND_RESPIRATORY_ELECTRON_TRANSPORT</b>	9.30E-16	2.40E-13	174	24
REACTOME_NEURONAL_SYSTEM	3.00E-15	6.70E-13	398	34
REACTOME_INTRA_GOLGI_AND_RETROGRADE_GOLGI_TO_ER_TRAFFIC	1.10E-14	2.20E-12	194	24
REACTOME_METABOLISM_OF_LIPIDS	1.40E-14	2.30E-12	723	45
REACTOME_ANTIGEN_PROCESSING_UBIQUITINATION_PROTEASOME_DEGRADATION	9.30E-13	1.40E-10	305	27
REACTOME_CLASS_I_MHC_MEDIATED_ANTIGEN_PROCESSING_PRESENTATION	1.40E-12	2.00E-10	360	29
<b>REACTOME_PYRUVATE_METABOLISM_AND_CITRIC_ACID_TCA_CYCLE</b>	2.30E-12	2.90E-10	54	13
REACTOME_ASPARAGINE_N_LINKED_GLYCOSYLATION	4.00E-12	4.70E-10	300	26
REACTOME_TRANSMISSION_ACROSS_CHEMICAL_SYNAPSES	7.00E-12	7.80E-10	260	24
REACTOME_TRANSPORT_TO_THE_GOLGI_AND_SUBSEQUENT_MODIFICATION	1.70E-11	1.70E-09	182	20
REACTOME_DISEASE	2.30E-11	2.10E-09	1481	61
REACTOME_GOLGI_TO_ER_RETROGRADE_TRANSPORT	2.30E-11	2.10E-09	127	17
REACTOME_ION_CHANNEL_TRANSPORT	9.70E-11	8.40E-09	179	19
REACTOME_PROTEIN_LOCALIZATION	1.70E-10	1.40E-08	164	18
REACTOME_GABA_SYNTHESIS_RELEASE_REUPTAKE_AND_DEGRADATION	2.50E-10	2.00E-08	19	8

Important categories highlighted in the main text are shown in bold.

RNA molecules stably across corticogenesis, a substantial portion of the cargo changed in a dynamic manner. The dynamic cargo includes pro-IPC determinants and cortical layer markers, consistent with a role for STAU2 in distributing transcripts that regulate production of specific types of progeny. To our knowledge, this is the first study to describe temporal changes in target RNA molecules bound by an individual RBP during development. Our findings indicate that delivery of a complex targetome by STAU2 into IPCs that changes during development may contribute to cell fate specification and differentiation during the span of corticogenesis.

Previously, RIP analyses utilizing microarrays have shown that STAU2 can bind large numbers of RNA molecules. For example, 1206 target mRNAs were detected in lysates from E17 rat brain (Heraud-Farlow et al., 2013), 1566 targets in the E13-E14 cortex (Kusek et al., 2012), and approximately 2000 targets were detected in STAU2-transfected human embryonic kidney (HEK) 293 T cells (Furic et al., 2007). Our analysis identified a total of 18,975 peaks corresponding to 7968 genes. This difference in STAU2 cargo size could be due to several factors, such as use of RNA sequencing instead of microarrays to identify targets, the peak calling-based cargo identification method, or the greater variety of transcripts revealed by assessing four time points. Other studies using CLIP or modified RIP protocols followed by RNA-seq have similarly identified several thousand genes bound to other RBPs. For example, 15,000-20,000 binding sites corresponding to 4000-5000 genes were identified for HuR at a single time point (Lebedeva et al., 2011), ~6000 genes were found to interact with FMRP in HEK293 cells (Ascano et al., 2012), and 14,376 peaks in the mouse brain (Maurin et al., 2018) where a similar peak identification method was used. Hence, advances in methods of detection and analysis are demonstrating the complexity of RBP targetomes and the central role these molecules play in RNA localization and regulation in different cellular contexts.

Our RIP-seq dataset contains several previously validated STAU2 targets, such as *Camk2a* (Fritzsche et al., 2013), *Sacm11*, *Calm3*, *Rgs2*, *Stx1a*, *Nnat*, *Actg1* (Heraud-Farlow et al., 2013), *Hes6*, *Cdh5* and *Mkks* (Kusek et al., 2012). Other targets, such as *Rgs4* in rat brain (Heraud-Farlow et al., 2013) and *Prox1* in mouse cortex (Vessey et al., 2012), were not detected, possibly owing to

technical differences, analytical approaches or species differences. Nevertheless, at a more global level, we confirmed that STAU2 binds transcripts associated with several processes and pathways important for brain development, such as cell cycle, neurogenesis, protein localization and RNA processing (Kusek et al., 2012; Heraud-Farlow et al., 2013), and extended these studies by demonstrating significantly greater cargo complexity. Moreover, we were able to gain further insight into STAU2 function by classifying the cargo into stable or dynamic, based on the detected transcripts bound over time.

In accordance with previous studies implicating RBPs in regulation of basic cellular events (Gerstberger et al., 2014), stable genes in the STAU2 cargo were associated with processes and pathways, such as chromosome organization, macromolecule localization, translation, mRNA splicing and DNA repair, that likely occur throughout neurogenesis. However, STAU2 is also involved in processes that vary during cortical development, such as dendritic spine morphogenesis (Goetze et al., 2006) and synaptogenesis (Berger et al., 2017; Pernice et al., 2019). Indeed, dynamic genes showed enrichment in categories related to neurogenesis, cell projection organization, transmission across chemical synapses, neurotransmitter release and neurite outgrowth. This dynamicity in the cargo may be due to several factors, such as altered gene expression over time, altered modification of RNAs that changes their binding affinity to STAU2, or alterations in STAU2 protein expression, modification, protein-protein interactions or localization.

Of the Reactome parent pathways identified, 'extracellular matrix (ECM) proteins' was exclusively enriched in the dynamic gene set. Although ECM proteins provide structural support, they also modulate signaling pathways that drive proliferation and neurogenesis (Long and Huttner, 2019). Proteoglycans are major constituents of the ECM and cell surfaces in the brain and serve as dynamic fields of signaling that regulate cell behavior; ECM dynamics are important for cell growth, differentiation and migration (Maeda, 2015; Schwartz and Domowicz, 2018). Genes coding for proteoglycans, such as *Bcan* (brevican), *Ptprz1* (phosphocan), *Bgn* (biglycan), *Dcn* (decorin), *Vtn* (vitronectin), *Lum* (lumican), *Ncan*, *Ptprs* and *Gpc4* were enriched in the dynamic

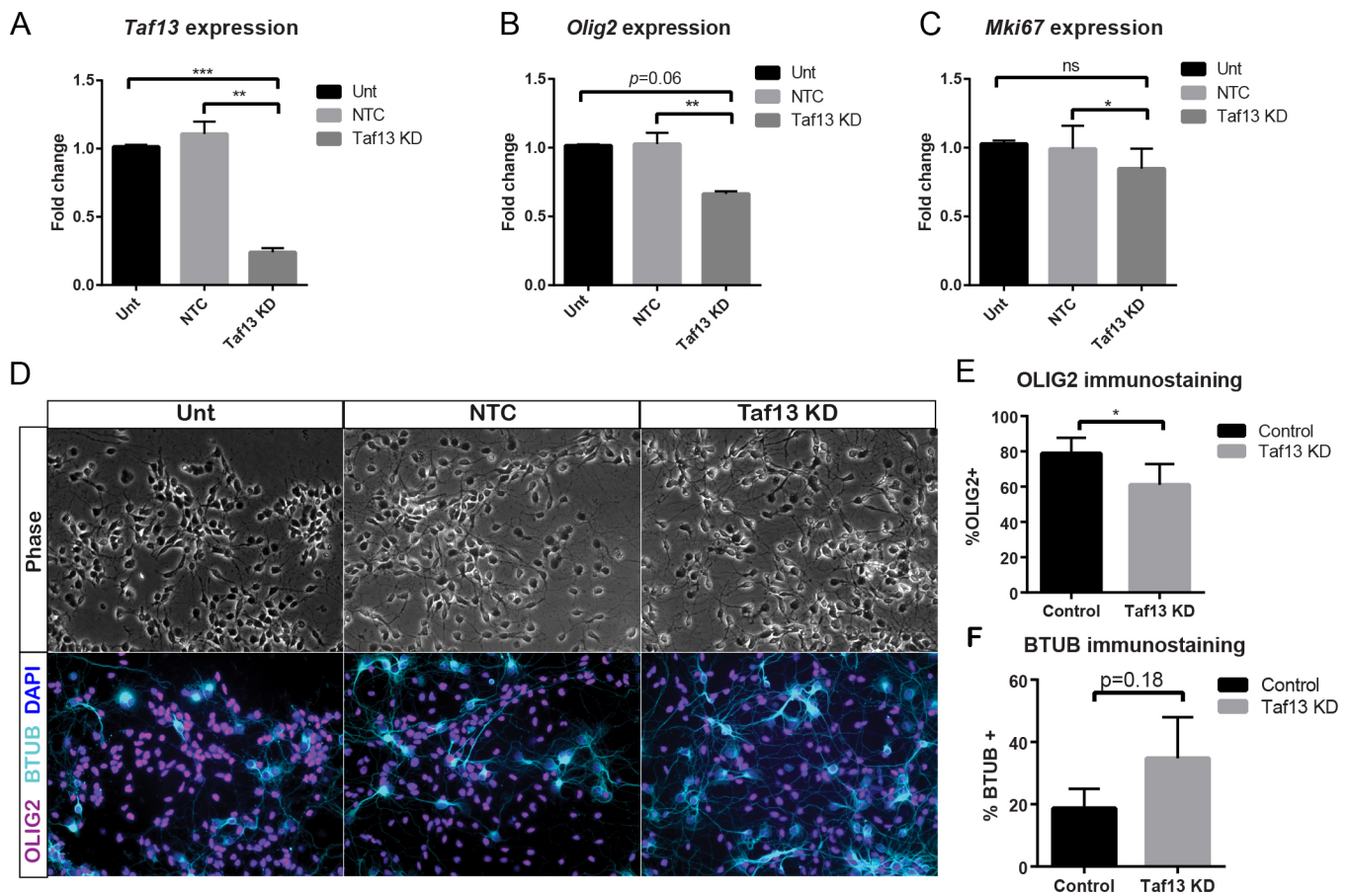


**Fig. 6. Knockdown of a STAU2 target, *Taf13*, reduces OLIG2<sup>+</sup> cells.** (A–C) E13.5 mouse cortical cells *in vitro* were infected with shRNAs targeting *Taf13* or NTC shRNA at MOI=3, and cultured for 5 DIV. qRT-PCR was used to quantify (A) *Taf13*, (B) *Mki67* and (C) *Olig2* expression. (D) Representative images showing phase-contrast images, and DAPI, OLIG2 and BTUB immunostaining in E13.5+5DIV mouse cortical cultures. (E,F) Quantification of OLIG2<sup>+</sup> (E) and BTUB<sup>+</sup> (F) cells as a percentage of total DAPI<sup>+</sup> cells. NTC, non-targeting control virus; TAF13 KD, infection with a combination of two *Taf13*-targeting shRNAs; Unt, untreated. \* $P < 0.05$ , paired Student's *t*-test,  $n = 3$ . ns, not significant. Graphs show mean  $\pm$  s.e.m. See also Fig. S6.

cargo. The interaction of STAU2 with specific ECM-related genes could have important implications for development and disease. For example, loss of function of the cargo proteoglycans *Bcan* and *Ndst1* leads to impaired hippocampal LTP (Bülow and Hobert, 2006), axon guidance defects and autism, and intellectual disability and epilepsy, respectively (Maeda, 2015). A number of integrins were enriched in the cargo, including *Itgb1bp1*, *Itga4*, *Itga6*, *Itga9* and *Itga11*. Integrins modulate and drive signaling pathways that regulate proliferation and differentiation during early development, and neocortex size and folding during late neural development (Long and Huttner, 2019; Milner and Campbell, 2002). For example, disruption of integrin  $\alpha 6$  (*Itga6*) caused abnormal cortical plate lamination (Barros et al., 2011).

In the Reactome parent pathway ‘nervous system development’, some branches under the ‘axon guidance’ subdivision, such as EPH-Ephrin signaling, were associated with the partially dynamic and stable groups, whereas others, such as NCAM1 signaling for neurite outgrowth, were only enriched in the dynamic group. Similarly, for the ‘autophagy’ parent pathway, whereas dynamic genes were associated only with aggrephagy (the selective recognition and subsequent degradation of protein aggregates; Malampati et al., 2020), stable genes were involved in both aggrephagy and mitophagy. The identification of pathways not previously associated with STAU2 cargo, including ECM regulation, autophagy, aggrephagy, lipid and carbohydrate metabolism, and the

fact that some functions appear regulated in a highly dynamic manner, encourage future investigations into other previously unidentified roles for STAU2 in brain development and function.

Given the specific inheritance of STAU2 by IPCs during asymmetric cell divisions, we reasoned that STAU2 cargo inheritance may promote the IPC fate. Indeed, approximately one-third of all pro-IPC genes identified by Aprea et al. (2013) were enriched in the STAU2 cargo, with a higher magnitude of binding at E13.5 and E15.5, correlating with the peak timing of IPC generation (Haubensack et al., 2004; Miyata et al., 2004). We found a similar enrichment in DB factors in the cargo at these stages (SVZ-DB), including several known IPC markers, such as *Tbr2* (Englund et al., 2005), *Gadd45g*, *Mfng*, *Hes6*, *Sdc3*, *Slc17a6*, *Elavl4*, *Cxcl12*, *Sorbs2*, *Serping1*, *Nrn1*, *Myt1*, *Neurod1* (Kawaguchi et al., 2008), *Cux1* (Nieto et al., 2004) and *Scrt2* (Paul et al., 2014) (Table S1). This supports a role for STAU2 in delivering a complex of molecules that act as IPC determinants to promote the transition of RGCs to IPCs.

IPCs produce DL and UL neurons in temporal order (Mihalas et al., 2016; Hevner, 2019). Our analysis showed that markers of DL neurons peaked in the cargo at E15.5 and declined at E17.5, whereas markers of UL neurons were lower than DL genes at E13.5 and E15.5, and higher at E17.5. Hence, the dynamic nature of STAU2-bound cargo could be important for conferring progenitors with specific neuronal identity. Enrichment analysis of a comprehensive list of cortical layer markers also implicated STAU2 in cortical neuron

layer specification. Notably, layer V genes in the cargo were associated with cellular metabolism-linked pathways. The large layer V pyramidal neurons are the only cell types in the cortex to project beyond the skull (Guillemot et al., 2006), with higher soma area and axon length than cells in layers II, III and IV (Wang et al., 2018) and high metabolic demands (Agostini et al., 2016; Belgard et al., 2011). The prevalence of pathways related to metabolism observed for layer V cells in the dynamic cargo fit with a scenario of evolving metabolic needs as these cells differentiate to attain and then maintain their specific morphology and extensive projections. Moreover, metabolic dysregulation is a feature of many diseases, such as amyotrophic lateral sclerosis (Vandoorne et al., 2018), Parkinson's disease (Błaszczyk, 2018) and Alzheimer's disease (Wang et al., 2020), which preferentially affect cells with long axons and high metabolic demands. The presence of these metabolism- and disease-related genes in the cargo, together with our observation that STAU2 is more highly expressed in BCL11B<sup>+</sup> layer V cells than other layers in both embryonic (E17.5) and adult cortices, implicates STAU2 in the proper growth and survival of these cells. In the future, it will be worthwhile investigating whether metabolism in layer V projection neurons is particularly affected by loss of STAU2 function.

One of our predictions was that deeper analysis of the STAU2 cargo would reveal previously unidentified determinants of cortical cell fate. Among the STAU2 targets was a transcript for TAF13, which, with TAF11, is recruited to the RNA polymerase II general transcription factor (TFIID) complex. After *Taf13* KD in cortical progenitor cells *in vitro*, we observed a significant decrease in *Olig2* expression and in the number of OLIG2<sup>+</sup> cells and a trend towards increased BTUB<sup>+</sup> cells. We also observed elevated *Olig2* transcript levels in the STAU2 cargo at E17.5, corresponding to the onset of oligodendrogenesis (Kessaris et al., 2006; Kriegstein and Alvarez-Buylla, 2009). *Taf13* is a target of OLIG2 in the mouse spinal cord (Darr et al., 2017) suggesting a potential co-regulatory relationship. Mutations in *Taf13* have also been linked to delayed myelination, microcephaly and growth retardation in humans (Tawamie et al., 2017), which corroborates our findings of reduced oligodendrocyte production and reduced progenitor proliferation after KD. These results provide insight into how STAU2, by regulating transcription factors such as TAF13, may control not only RGC-IPC-neuronal transitions but also neuronal-glial fate switches. Furthermore, we note that other TFs involved in gliogenesis, including *Nfia*, *Sox10* and *Olig2* (Table S1), are enriched in the STAU2 cargo at later stages.

In conclusion, this temporal RIP-seq analysis expands our understanding of STAU2 function in the developing cortex, highlights stable and dynamic subsets of genes in the cargo, and forms a foundation for further study of how newly revealed candidate determinants and pathways contribute to orderly corticogenesis.

## MATERIALS AND METHODS

### Mice (*Mus musculus*)

Swiss Webster (SW) mice were obtained as timed pregnant females (Taconic Biosciences). Both male and female mice were included and all experiments were performed in accordance with protocols approved by the Institutional Animal Care and Use Committee (IACUC) at the University of Albany, Albany, NY, USA.

### RIP

RIP experiments were performed as described previously (Baroni et al., 2008; Kusek et al., 2012; Tenenbaum et al., 2002). Pooled cortical tissue from a litter of embryos was used as starting material for each independent experiment (i.e. biological replicate). For each RIP, 10 µg of anti-STAU2 (Abcam, ab60724) was mixed with 50 µl Dynabeads Protein G (Invitrogen). A magnetic rack (Millipore) was used for the washing steps. RNA was

isolated and purified with acid phenol/chloroform extraction. For generation of the RIP-seq dataset, STAU2 RIP results were compared directly to input samples. Previous RIP experiments using the same antibodies showed that negative control T7 antibody RIPs had only trace RNA bound and were not useful to distinguish selective enrichment, so were not included in this analysis; rather, we used the peak-calling method over input to determine selective enrichment. After generation of the RIP-seq dataset, targets were chosen for validation using qPCR. For this, RIPs were performed with the MAGNA-RIP kit (Millipore, 17-700). For each RIP, 50 µl of Protein A/G beads were blocked with 2% UltraPure BSA (Thermo Fisher, AM2616) at room temperature (RT) for 1–2 h before overnight incubation with 10 µg mouse monoclonal anti-STAU2 antibody (gift from Michael Kiebler, Ludwig-Maximilians-University, Germany) or mouse IgG (MAGNA-RIP kit) antibodies. RNA was purified using TRIzol (Thermo Fisher) and RNA Clean and Concentrator (Zymo Research, R1014) kits, with DNase treatment.

### Library preparation for RNA-seq

Total RNA (input) and RNA samples purified after STAU2 RIP (described above) were used for RNA-seq. The libraries were prepared using ScriptSeq Complete Kit (Human/Mouse/Rat)-Low Input (Epicentre/Illumina, SCL24H) following the manufacturer's instructions. Briefly, a maximum of 800 ng of DNA-free RNA was used for ribosomal RNA removal using Ribo-Zero rRNA removal kit. rRNA-free samples were used for ScriptSeq v2 RNA-seq library preparation, which included RNA fragmentation, cDNA synthesis and terminal tagging. Purified cDNAs were PCR amplified using ScriptSeq Index PCR Primers (Epicentre/Illumina, RSBC10948) to barcode the libraries for multiplexing according to the manufacturer's instructions. After final purification, the libraries were sent to the UB Next-Generation Sequencing and Expression Analysis Core at SUNY Buffalo for quality checks and high-throughput sequencing (single-end) using the Illumina platform.

### RIP-seq and bioinformatic analysis

Detailed code is provided at: <https://github.com/neural-stem-cell-institute/Stau2>. FASTQ files for triplicate STAU2 RIP and input control samples were mapped to the mm10 genome using STAR (version 2.5). Peaks were called using the FindPeaks function in Homer (version 4.10) to identify statistically enriched peaks with a 4-fold enrichment over input and common across replicates. We filtered the peaks based on the Peak Scores provided by HOMER by calculating the elbow point and taking the peaks with higher scores. Then using the GenomicRanges and GenomicAlignments packages in R, the reads associated with either the positive or negative strand at the identified peak locations were counted to generate a counts matrix, and stranded positions with fewer than five counts were dropped from further analysis. The count matrix was normalized through an iterative resampling algorithm that provides ~10 million reads per sample. Each position was then annotated in R using the gencode annotation for mouse (M21) while retaining strand-specific data.

We next sought to identify those genes that differentially bound STAU2 over the time course. We developed an algorithm that calculates a Bayes factor indicating the likelihood of changing over the time course. Briefly, peaks within a gene were selected and weighted according to the Peak score, then a t-statistic was calculated from the normalized counts between time-points and a ln Bayes factor [ln(BF)] was derived using the BayesFactor package for each comparison and summed over the time course. Genes were then classified as dynamic [ln(BF)>4.61], partially dynamic, or stable [ln(BF)<1.163] cargo and enrichment analysis was carried out using the hyper package. Detailed description of other computational analyses may be found in supplementary Materials and Methods and at <https://github.com/neural-stem-cell-institute/Stau2>.

### Immunohistochemistry (IHC) and imaging

Mouse brains were fixed overnight at 4°C in 4% paraformaldehyde (Santa Cruz Biotechnology) or PHEM-fix (Bowser and Rieder, 1985). Tissue was washed three times with PBS, equilibrated in 30% sucrose at 4°C for approximately 48 h and frozen in optimal cutting temperature (OCT) compound (Sakura Finetek) before storage at –80°C. Coronal cryostat sections were cut at a thickness of 20 µm. Samples were blocked at RT for 60

mins with a 0.3% Triton-X/PBS solution containing 3% bovine serum albumin (BSA) and 2% goat serum (Jackson ImmunoResearch), before overnight incubation at 4°C with primary antibody (Table S12). Alexa Fluor 488, 594 and 647 (Thermo Fisher), as well as Cy3 (Jackson ImmunoResearch) conjugated, species-specific secondary antibodies, were used at a dilution of 1:300. DAPI (4',6-diamidino-2-phenylindole) was used at a dilution of 1:1000 for nuclear staining. Prolong Gold antifade reagent (Invitrogen, P36930) was used for mounting sections on glass slides. Tissue sections were imaged on a Zeiss LSM 780 confocal microscope.

### Cortical cell culture

Cerebral cortices were dissociated by trituration and enzymatic digestion (30 min at 37°C) in a DMEM (Thermo Fisher) solution containing 50 units of Papain (Worthington Biochemical Corporation), 24 µg/ml DNase I (Sigma-Aldrich), 2 mM L-glutamine (Thermo Fisher), 1 mM N-acetyl-L-cysteine (NAC; Sigma-Aldrich) and 1 mM sodium pyruvate (Thermo Fisher). After dissociation, cells were rinsed three times with DMEM, triturated to yield a largely single-cell suspension, plated on PLL-coated surfaces (24-well plate, Corning) and cultured in serum-free medium containing DMEM, N2 (Thermo Fisher), B27 (Thermo Fisher), 2 mM L-glutamine (Thermo Fisher), 1 mM sodium pyruvate (Thermo Fisher), 1 mM NAC (Sigma-Aldrich) and 10 ng/ml FGF2 (Thermo Fisher). The culture medium was filtered at 0.22 µm, and culture medium was changed every 2 days.

### Lentiviral vector production and infection

For *Taf13* KD experiments, shRNA lentiviral plasmids were purchased from Sigma-Aldrich [TAF13 MISSION shRNA Bacterial Glycerol Stock (mouse) SHCLNG-NM\_025444 and MISSION pLKO.1-puro Non-Mammalian shRNA Control Plasmid DNA]. 293FT cells were co-transfected with packaging plasmids pCMV-VSVG and pCMV-dvpr, using polyethylenimine. Viral supernatants were collected 48 and 72 h post-transfection, concentrated with LentiX Concentrator (Clontech), and titered via qPCR (ABM qPCR Lentivirus Titration Kit) before storage at -80°C. For infection, *Taf13* shRNA and non-targeting control (NTC) lentiviral vectors were added to cells immediately before plating at a multiplicity of infection (MOI) of 3 and removed after 36 h. STAU2 KD experiments were performed as described by Kusek et al., 2012.

### Quantitative real-time PCR (qPCR)

cDNA synthesis was performed with the Superscript VILO kit (Thermo Fisher, 11754050). POWER SYBR Green Master Mix (Thermo Fisher, 4367659) was used to perform qPCR. Primers (IDT) were designed using the Primer3 software to produce amplicons of 100–200 bp targeted to genomic regions identified as peaks, amplifying either coding or 3'UTR sequences (Table S12). The comparative Ct method ( $\Delta\Delta C_t$ ) was used to determine relative expression, with primer pairs tested for similar efficiency. All reactions were run on a QuantStudio 6 Flex Real-Time PCR System.

### Acknowledgements

We thank Michael Kiebler (Medical Faculty, LMU Muenchen, Germany) for the generous gift of the monoclonal anti-STAU2 antibody and for helpful discussions.

### Competing interests

The authors declare no competing or financial interests.

### Author contributions

Conceptualization: R.C., F.D., S.A.T., G.K., S.A., N.C.B., S.T.; Methodology: R.C., Y.W., M.C., S.K.G., F.D., S.A.T., G.K., T.R.K., S.A., N.C.B., S.T.; Software: R.C., T.R.K., N.C.B.; Validation: R.C., Y.W., M.C., S.K.G., S.A., N.C.B., S.T.; Formal analysis: R.C., S.K.G., F.D., S.A.T., T.R.K., S.A., N.C.B., S.T.; Investigation: R.C., Y.W., M.C., G.K., S.A., N.C.B., S.T.; Resources: R.C., G.K., S.T.; Data curation: R.C., F.D., S.A.T., T.R.K., S.A., N.C.B.; Writing - original draft: R.C., S.A., N.C.B., S.T.; Writing - review & editing: R.C., Y.W., M.C., S.K.G., F.D., S.A.T., G.K., T.R.K., S.A., N.C.B., S.T.; Visualization: R.C., N.C.B., S.T.; Supervision: S.A., N.C.B., S.T.; Project administration: S.T.; Funding acquisition: S.A., S.T.

### Funding

This work was supported by the National Institute of Neurological Disorders and Stroke [R35 NS097277 to S.T.]. Deposited in PMC for release after 12 months.

### Data availability

RIP-seq data have been deposited in Gene Expression Omnibus under accession number GSE163378, and Homer code is available at <https://github.com/neural-stem-cell-institute/Stau2>.

### Peer review history

The peer review history is available online at <https://journals.biologists.com/dev/article-lookup/doi/10.1242/dev.199376>

### References

- Agostini, M., Romeo, F., Inoue, S., Niklison-Chirou, M. V., Elia, A. J., Dinsdale, D., Morone, N., Knight, R. A., Mak, T. W. and Melino, G. (2016). Metabolic reprogramming during neuronal differentiation. *Cell Death Differ.* **23**, 1502–1514. doi:10.1038/cdd.2016.36
- Apnea, J., Prenninger, S., Dori, M., Ghosh, T., Monasor, L. S., Wessendorf, E., Zocher, S., Massalini, S., Alexopoulou, D., Lesche, M. et al. (2013). Transcriptome sequencing during mouse brain development identifies long non-coding RNAs functionally involved in neurogenic commitment. *EMBO J.* **32**, 3145–3160. doi:10.1038/emboj.2013.245
- Ascano, M., Jr, Mukherjee, N., Bandaru, P., Miller, J. B., Nusbaum, J. D., Corcoran, D. L., Langlois, C., Munschauer, M., Dewell, S., Hafner, M. et al. (2012). FMRP targets distinct mRNA sequence elements to regulate protein expression. *Nature* **492**, 382–386. doi:10.1038/nature11737
- Baroni, T. E., Chittur, S. V., George, A. D. and Tenenbaum, S. A. (2008). Advances in RIP-chip analysis: RNA-binding protein immunoprecipitation-microarray profiling BT - Post-transcriptional gene regulation. In (ed. J. Wilusz), pp. 93–108. Totowa, NJ: Humana Press.
- Barros, C. S., Franco, S. J. and Müller, U. (2011). Extracellular matrix: functions in the nervous system. *Cold Spring Harb. Perspect. Biol.* **3**, a005108. doi:10.1101/cshperspect.a005108
- Belgard, T. G., Marques, A. C., Oliver, P. L., Abaan, H. O., Sirey, T. M., Hoerder-Suabedissen, A., García-Moreno, F., Molnár, Z., Margulies, E. H. and Ponting, C. P. (2011). A transcriptomic atlas of mouse neocortical layers. *Neuron* **71**, 605–616. doi:10.1016/j.neuron.2011.06.039
- Berger, S. M., Fernández-Lamo, I., Schöning, K., Fernández Moya, S. M., Ehses, J., Schieweck, R., Clementi, S., Enkel, T., Grothe, S., von Bohlen und Halbach, O. et al. (2017). Forebrain-specific, conditional silencing of *Staufen2* alters synaptic plasticity, learning, and memory in rats. *Genome Biol.* **18**, 222. doi:10.1186/s13059-017-1350-8
- Betancourt, J., Katzman, S. and Chen, B. (2014). Nuclear factor one B regulates neural stem cell differentiation and axonal projection of corticofugal neurons. *J. Comp. Neurol.* **522**, 6–35. doi:10.1002/cne.23373
- Błaszczak, J. W. (2018). The emerging role of energy metabolism and neuroprotective strategies in Parkinson's disease. *Front. Aging Neurosci.* **10**, 301. doi:10.3389/fnagi.2018.00301
- Bowser, S. S. and Rieder, C. L. (1985). Evidence that cell surface motility in *Allogromia* is mediated by cytoplasmic microtubules. *Can. J. Biochem. Cell Biol.* **63**, 608–620. doi:10.1139/o85-079
- Britanova, O., de Juan Romero, C., Cheung, A., Kwan, K. Y., Schwark, M., Gyorgy, A., Vogel, T., Akopov, S., Mitkovski, M., Agoston, D. et al. (2008). *Satb2* is a postmitotic determinant for upper-layer neuron specification in the neocortex. *Neuron* **57**, 378–392. doi:10.1016/j.neuron.2007.12.028
- Broadus, J., Fuerstenberg, S. and Doe, C. Q. (1998). *Staufen*-dependent localization of prospero mRNA contributes to neuroblast daughter-cell fate. *Nature* **391**, 792–795. doi:10.1038/35861
- Buchner, G., Bassi, M. T., Andolfi, G., Ballabio, A. and Franco, B. (1999). Identification of a novel homolog of the *Drosophila* *staufen* protein in the chromosome 8q13–q21.1 Region. *Genomics* **62**, 113–118. doi:10.1006/geno.1999.6015
- Bülow, H. E. and Hobert, O. (2006). The molecular diversity of glycosaminoglycans shapes animal development. *Annu. Rev. Cell Dev. Biol.* **22**, 375–407. doi:10.1146/annurev.cellbio.22.010605.093433
- Cadwell, C. R., Bhaduri, A., Mostajo-Radji, M. A., Keefe, M. G. and Nowakowski, T. J. (2019). Development and arealization of the cerebral cortex. *Neuron* **103**, 980–1004. doi:10.1016/j.neuron.2019.07.009
- Chen, B., Schaevitz, L. R. and McConnell, S. K. (2005). *Fez1* regulates the differentiation and axon targeting of layer 5 subcortical projection neurons in cerebral cortex. *Proc. Natl. Acad. Sci. USA* **102**, 17184–17189. doi:10.1073/pnas.0508732102
- Chen, H.-R., Juan, H.-C., Wong, Y.-H., Tsai, J.-W. and Fann, M.-J. (2017a). *Cdk12* regulates neurogenesis and late-arising neuronal migration in the developing cerebral cortex. *Cereb. Cortex* **27**, 2289–2302.
- Chen, L., Jensik, P. J., Alaimo, J. T., Walkiewicz, M., Berger, S., Roeder, E., Faqeh, E. A., Bernstein, J. A., Smith, A. C. M., Mullegama, S. V. et al. (2017b). Functional analysis of novel DEAF1 variants identified through clinical exome sequencing expands DEAF1-associated neurodevelopmental disorder (DAND) phenotype. *Hum. Mutat* **38**, 1774–1785. doi:10.1002/humu.23339
- Cubelos, B., Sebastián-Serrano, A., Beccari, L., Calcagnotto, M. E., Cisneros, E., Kim, S., Dopazo, A., Alvarez-Dolado, M., Redondo, J. M., Bovolenta, P.

- et al. (2010). Cux1 and Cux2 regulate dendritic branching, spine morphology, and synapses of the upper layer neurons of the cortex. *Neuron* **66**, 523-535. doi:10.1016/j.neuron.2010.04.038
- Darr, A. J., Danzi, M. C., Brady, L., Emig-Agius, D., Hackett, A., Golshani, R., Warner, N., Lee, J., Lemmon, V. P. and Tsoulfas, P. (2017). Identification of genome-wide targets of Olig2 in the adult mouse spinal cord using ChIP-Seq. *PLoS ONE* **12**, e0186091.
- Duchaine, T. F., Hemraj, I., Furic, L., Deitinghoff, A., Kiebler, M. A. and DesGroseillers, L. (2002). Stau2 isoforms localize to the somatodendritic domain of neurons and interact with different organelles. *J. Cell Sci.* **115**, 3285-3295. doi:10.1242/jcs.115.16.3285
- Easter, S. S. J., Ross, L. S. and Frankfurter, A. (1993). Initial tract formation in the mouse brain. *J. Neurosci.* **13**, 285-299. doi:10.1523/JNEUROSCI.13-01-00285.1993
- Englund, C., Fink, A., Lau, C., Pham, D., Daza, R. A. M., Bulfone, A., Kowalczyk, T. and Hevner, R. F. (2005). Pax6, Tbr2, and Tbr1 are expressed sequentially by radial glia, intermediate progenitor cells, and postmitotic neurons in developing neocortex. *J. Neurosci.* **25**, 247-251. doi:10.1523/JNEUROSCI.2899-04.2005
- Fame, R. M., MacDonald, J. L., Dunwoodie, S. L., Takahashi, E. and Macklis, J. D. (2016). Cited2 regulates neocortical layer II/III generation and somatosensory callosal projection neuron development and connectivity. *J. Neurosci.* **36**, 6403-6419. doi:10.1523/JNEUROSCI.4067-15.2016
- Fietz, S. A., Lachmann, R., Brandl, H., Kircher, M., Samusik, N., Schröder, R., Lakshmanaperumal, N., Henry, I., Vogt, J., Riehn, A. et al. (2012). Transcriptomes of germinal zones of human and mouse fetal neocortex suggest a role of extracellular matrix in progenitor self-renewal. *Proc. Natl. Acad. Sci. USA* **109**, 11836-11841. doi:10.1073/pnas.1209647109
- Fritzsche, R., Karra, D., Bennett, K. L., Ang, F. Y., Heraud-Farlow, J. E., Tolino, M., Doyle, M., Bauer, K. E., Thomas, S., Planavsky, M. et al. (2013). Interactome of two diverse RNA granules links mRNA localization to translational repression in neurons. *Cell Rep* **5**, 1749-1762. doi:10.1016/j.celrep.2013.11.023
- Furic, L., Maher-Laporte, M. and DesGroseillers, L. (2007). A genome-wide approach identifies distinct but overlapping subsets of cellular mRNAs associated with Stau1- and Stau2-containing ribonucleoprotein complexes. *RNA* **14**, 324-335. doi:10.1261/ma.720308
- Gerstberger, S., Hafner, M. and Tuschl, T. (2014). A census of human RNA-binding proteins. *Nat. Rev. Genet.* **15**, 829-845. doi:10.1038/nrg3813
- Goetze, B., Tuebing, F., Xie, Y., Dorostkar, M. M., Thomas, S., Pehl, U., Boehm, S., Macchi, P. and Kiebler, M. A. (2006). The brain-specific double-stranded RNA-binding protein Stau2 is required for dendritic spine morphogenesis. *J. Cell Biol.* **172**, 221-231. doi:10.1083/jcb.200509035
- Gopalan, S. M., Wilczynska, K. M., Konik, B. S., Bryan, L. and Kordula, T. (2006). Nuclear factor-1X regulates astrocyte-specific expression of the alpha1-antichymotrypsin and glial fibrillary acidic protein genes. *J. Biol. Chem.* **281**, 13126-13133. doi:10.1074/jbc.M601194200
- Gorski, J. A., Talley, T., Qiu, M., Puelles, L., Rubenstein, J. L. R. and Jones, K. R. (2002). Cortical excitatory neurons and glia, but not GABAergic neurons, are produced in the Emx1-expressing lineage. *J. Neurosci.* **22**, 6309-6314. doi:10.1523/JNEUROSCI.22-15-06309.2002
- Götz, M. and Barde, Y.-A. (2005). Radial glial cells defined and major intermediates between embryonic stem cells and CNS neurons. *Neuron* **46**, 369-372. doi:10.1016/j.neuron.2005.04.012
- Götz, M., Stoykova, A. and Gruss, P. (1998). Pax6 controls radial glia differentiation in the cerebral cortex. *Neuron* **21**, 1031-1044. doi:10.1016/S0896-6273(00)80621-2
- Guillemot, F., Molnár, Z., Tarabykin, V. and Stoykova, A. (2006). Molecular mechanisms of cortical differentiation. *Eur. J. Neurosci.* **23**, 857-868. doi:10.1111/j.1460-9568.2006.04626.x
- Hansel, C. (2019). Deregulation of synaptic plasticity in autism. *Neurosci. Lett.* **688**, 58-61. doi:10.1016/j.neulet.2018.02.003
- Haubensak, W., Attardo, A., Denk, W. and Huttner, W. B. (2004). Neurons arise in the basal neuroepithelium of the early mammalian telencephalon: a major site of neurogenesis. *Proc. Natl. Acad. Sci. USA* **101**, 3196-3201. doi:10.1073/pnas.0308600100
- Heinz, S., Benner, C., Spann, N., Bertolino, E., Lin, Y. C., Laslo, P., Cheng, J. X., Murre, C., Singh, H. and Glass, C. K. (2010). Simple combinations of lineage-determining transcription factors prime cis-regulatory elements required for macrophage and B cell identities. *Mol. Cell* **38**, 576-589. doi:10.1016/j.molcel.2010.05.004
- Hendzel, M. J., Wei, Y., Mancini, M. A., Van Hooser, A., Ranalli, T., Brinkley, B. R., Bazett-Jones, D. P. and Allis, C. D. (1997). Mitosis-specific phosphorylation of histone H3 initiates primarily within pericentromeric heterochromatin during G2 and spreads in an ordered fashion coincident with mitotic chromosome condensation. *Chromosoma* **106**, 348-360. doi:10.1007/s0044120050256
- Heraud-Farlow, J. E., Sharangdhar, T., Li, X., Pfeifer, P., Tauber, S., Orozco, D., Hörmann, A., Thomas, S., Bakosova, A., Farlow, A. R. et al. (2013). Stau2 regulates neuronal target RNAs. *Cell Rep* **5**, 1511-1518. doi:10.1016/j.celrep.2013.11.039
- Hevner, R. F. (2019). Intermediate progenitors and Tbr2 in cortical development. *J. Anat.* **235**, 616-625. doi:10.1111/joa.12939
- Hevner, R. F., Daza, R. A. M., Rubenstein, J. L. R., Stunnenberg, H., Olavarria, J. F. and Englund, C. (2003). Beyond laminar fate: toward a molecular classification of cortical projection/pyramidal neurons. *Dev. Neurosci.* **25**, 139-151. doi:10.1159/000072263
- Jayaseelan, S., Doyle, F., Currenti, S. and Tenenbaum, S. A. (2011). RIP: an mRNA localization technique. *Methods Mol. Biol.* **714**, 407-422. doi:10.1007/978-1-61779-005-8\_25
- Jeffreys, H. (1998). *The Theory of Probability*. OUP Oxford.
- Jhas, S., Ciura, S., Belanger-Jasmin, S., Dong, Z., Llamasos, E., Theriault, F. M., Joachim, K., Tang, Y., Liu, L., Liu, J. et al. (2006). Hes6 Inhibits Astrocyte Differentiation and Promotes Neurogenesis through Different Mechanisms. *J. Neurosci.* **26**, 11061-11071. doi:10.1523/JNEUROSCI.1358-06.2006
- Kang, P., Lee, H. K., Glasgow, S. M., Finley, M., Donti, T., Gaber, Z. B., Graham, B. H., Foster, A. E., Novitch, B. G., Gronostajski, R. M. et al. (2012). Sox9 and NFIA coordinate a transcriptional regulatory cascade during the initiation of gliogenesis. *Neuron* **74**, 79-94. doi:10.1016/j.neuron.2012.01.024
- Kawaguchi, A., Ikawa, T., Kasukawa, T., Ueda, H. R., Kurimoto, K., Saitou, M. and Matsuzaki, F. (2008). Single-cell gene profiling defines differential progenitor subclasses in mammalian neurogenesis. *Development* **135**, 3113-3124. doi:10.1242/dev.022616
- Kessaris, N., Fogarty, M., Iannarelli, P., Grist, M., Wegner, M. and Richardson, W. D. (2006). Competing waves of oligodendrocytes in the forebrain and postnatal elimination of an embryonic lineage. *Nat. Neurosci.* **9**, 173-179. doi:10.1038/nn1620
- Killen, A. C., Barber, M., Paulin, J. J. W., Ranscht, B., Parnavelas, J. G. and Andrews, W. D. (2017). Protective role of Cadherin 13 in interneuron development. *Brain Struct. Funct.* **222**, 3567-3585. doi:10.1007/s00429-017-1418-y
- Kowalczyk, T., Pontious, A., Englund, C., Daza, R. A. M., Bedogni, F., Hodge, R., Attardo, A., Bell, C., Huttner, W. B. and Hevner, R. F. (2009). Intermediate neuronal progenitors (basal progenitors) produce pyramidal-projection neurons for all layers of cerebral cortex. *Cereb. Cortex* **19**, 2439-2450. doi:10.1093/cercor/bhn260
- Kriegstein, A. and Alvarez-Buylla, A. (2009). The glial nature of embryonic and adult neural stem cells. *Annu. Rev. Neurosci.* **32**, 149-184. doi:10.1146/annurev.neuro.051508.135600
- Kusek, G., Campbell, M., Doyle, F., Tenenbaum, S. A., Kiebler, M. and Temple, S. (2012). Asymmetric segregation of the double-stranded RNA binding protein Stau2 during mammalian neural stem cell divisions promotes lineage progression. *Cell Stem Cell* **11**, 505-516. doi:10.1016/j.stem.2012.06.006
- Lebeau, G., Miller, L. C., Tartas, M., McAdam, R., Laplante, I., Badeaux, F., DesGroseillers, L., Sossin, W. S. and Lacaille, J.-C. (2011). Stau2 regulates mGluR long-term depression and Map1b mRNA distribution in hippocampal neurons. *Learn. Mem.* **18**, 314-326. doi:10.1101/lm.2100611
- Lebedeva, S., Jens, M., Theil, K., Schwanhäusser, B., Selbach, M., Landthaler, M. and Rajewsky, N. (2011). Transcriptome-wide analysis of regulatory interactions of the RNA-binding protein HuR. *Mol. Cell* **43**, 340-352. doi:10.1016/j.molcel.2011.06.008
- Lemke, J. R., Geider, K., Helbig, K. L., Heyne, H. O., Schütz, H., Hentschel, J., Courage, C., Depienne, C., Nava, C., Heron, D. et al. (2016). Delineating the GRIN1 phenotypic spectrum: a distinct genetic NMDA receptor encephalopathy. *Neurology* **86**, 2171-2178. doi:10.1212/WNL.0000000000002740
- Li, S., Zhang, C., Takemori, H., Zhou, Y. and Xiong, Z.-Q. (2009). TORC1 regulates activity-dependent CREB-target gene transcription and dendritic growth of developing cortical neurons. *J. Neurosci.* **29**, 2334-2343. doi:10.1523/JNEUROSCI.2296-08.2009
- Licatalosi, D. D., Mele, A., Fak, J. J., Ule, J., Kayikci, M., Chi, S. W., Clark, T. A., Schweitzer, A. C., Blume, J. E., Wang, X. et al. (2008). HITS-CLIP yields genome-wide insights into brain alternative RNA processing. *Nature* **456**, 464-469. doi:10.1038/nature07488
- Long, K. R. and Huttner, W. B. (2019). How the extracellular matrix shapes neural development. *Open Biol.* **9**, 180216. doi:10.1098/rsob.180216
- Loo, L., Simon, J. M., Xing, L., McCoy, E. S., Niehaus, J. K., Guo, J., Anton, E. S. and Zylka, M. J. (2019). Single-cell transcriptomic analysis of mouse neocortical development. *Nat. Commun.* **10**, 134. doi:10.1038/s41467-018-08079-9
- Maeda, N. (2015). Proteoglycans and neuronal migration in the cerebral cortex during development and disease. *Front. Neurosci.* **9**, 98. doi:10.3389/fnins.2015.00098
- Maher-Laporte, M. and DesGroseillers, L. (2010). Genome wide identification of Stau2-bound mRNAs in embryonic rat brains. *BMB Rep* **43**, 344-348. doi:10.5483/BMBRep.2010.43.5.344
- Malampati, S., Song, J.-X., Chun-Kit Tong, B., Nalluri, A., Yang, C.-B., Wang, Z., Gopalakrishna Sreenivasamurthy, S., Zhu, Z., Liu, J., Su, C. et al. (2020). Targeting aggrephagy for the treatment of Alzheimer's disease. *Cells* **9**, 311. doi:10.3390/cells9020311
- Malmevik, J., Petri, R., Klussendorf, T., Knauff, P., Åkerblom, M., Johansson, J., Soneji, S. and Jakobsson, J. (2015). Identification of the miRNA targetome in hippocampal neurons using RIP-seq. *Sci. Rep.* **5**, 12609. doi:10.1038/srep12609
- Matuzelski, E., Bunt, J., Harkins, D., Lim, J. W. C., Gronostajski, R. M., Richards, L. J., Harris, L. and Piper, M. (2017). Transcriptional regulation of Nfix by NFIB drives astrocytic maturation within the developing spinal cord. *Dev. Biol.* **432**, 286-297. doi:10.1016/j.ydbio.2017.10.019

- Maurin, T., Lebrigand, K., Castagnola, S., Paquet, A., Jarjat, M., Popa, A., Grossi, M., Rage, F. and Bardoni, B. (2018). HITS-CLIP in various brain areas reveals new targets and new modalities of RNA binding by fragile X mental retardation protein. *Nucleic Acids Res.* **46**, 6344-6355. doi:10.1093/nar/gky267
- Mihalas, A. B., Elsen, G. E., Bedogin, F., Daza, R. A. M., Ramos-Laguna, K. A., Arnold, S. J. and Hevner, R. F. (2016). Intermediate progenitor cohorts differentially generate cortical layers and require Tbr2 for timely acquisition of neuronal subtype identity. *Cell Rep.* **16**, 92-105. doi:10.1016/j.celrep.2016.05.072
- Milner, R. and Campbell, I. L. (2002). The integrin family of cell adhesion molecules has multiple functions within the CNS. *J. Neurosci. Res.* **69**, 286-291. doi:10.1002/jnr.10321
- Miyata, T., Kawaguchi, A., Saito, K., Kawano, M., Muto, T. and Ogawa, M. (2004). Asymmetric production of surface-dividing and non-surface-dividing cortical progenitor cells. *Development* **131**, 3133-3145. doi:10.1242/dev.01173
- Molyneaux, B. J., Ariotta, P., Hirata, T., Hibi, M. and Macklis, J. D. (2005). Fezl is required for the birth and specification of corticospinal motor neurons. *Neuron* **47**, 817-831. doi:10.1016/j.neuron.2005.08.030
- Moody, S. A., Quigg, M. S. and Frankfurter, A. (1989). Development of the peripheral trigeminal system in the chick revealed by an isotype-specific anti-beta-tubulin monoclonal antibody. *J. Comp. Neurol.* **279**, 567-580. doi:10.1002/cne.902790406
- Nicholson, C. O., Friedersdorf, M. and Keene, J. D. (2017). Quantifying RNA binding sites transcriptome-wide using DO-RIP-seq. *RNA* **23**, 32-46. doi:10.1261/rna.058115.116
- Nieto, M., Monuki, E. S., Tang, H., Imitola, J., Haubst, N., Khoury, S. J., Cunningham, J., Gotz, M. and Walsh, C. A. (2004). Expression of Cux-1 and Cux-2 in the subventricular zone and upper layers II-IV of the cerebral cortex. *J. Comp. Neurol.* **479**, 168-180. doi:10.1002/cne.20322
- Noctor, S. C., Martínez-Cerdeño, V., Ivic, L. and Kriegstein, A. R. (2004). Cortical neurons arise in symmetric and asymmetric division zones and migrate through specific phases. *Nat. Neurosci.* **7**, 136-144. doi:10.1038/nn1172
- Noctor, S. C., Martínez-Cerdeño, V. and Kriegstein, A. R. (2008). Distinct behaviors of neural stem and progenitor cells underlie cortical neurogenesis. *J. Comp. Neurol.* **508**, 28-44. doi:10.1002/cne.21669
- Novak, G., Zai, C. C., Mirkhani, M., Shaikh, S., Vincent, J. B., Meltzer, H., Lieberman, J. A., Strauss, J., Lévesque, D., Kennedy, J. L. et al. (2010). Replicated association of the NR4A3 gene with smoking behaviour in schizophrenia and in bipolar disorder. *Genes Brain Behav.* **9**, 910-917. doi:10.1111/j.1601-183X.2010.00631.x
- Ortiz, R., Georgieva, M. V., Gutiérrez, S., Pedraza, N., Fernández-Moya, S. M. and Gallego, C. (2017). Recruitment of Staufen2 enhances dendritic localization of an intron-containing CaMKII $\alpha$  mRNA. *Cell Rep.* **20**, 13-20. doi:10.1016/j.celrep.2017.06.026
- Parra-Damas, A., Valero, J., Chen, M., España, J., Martín, E., Ferrer, I., Rodríguez-Alvarez, J. and Saura, C. A. (2014). Crt1 activates a transcriptional program deregulated at early Alzheimer's disease-related stages. *J. Neurosci.* **34**, 5776-5787. doi:10.1523/JNEUROSCI.5288-13.2014
- Paul, V., Tonchev, A. B., Henningfeld, K. A., Pavlakis, E., Rust, B., Pieler, T. and Stoykova, A. (2014). Scratch2 Modulates neurogenesis and cell migration through antagonism of bHLH proteins in the developing neocortex. *Cereb. Cortex* **24**, 754-772. doi:10.1093/cercor/bhs356
- Penalva, L. O. F., Burdick, M. D., Lin, S. M., Sutterluety, H. and Keene, J. D. (2004). RNA-binding proteins to assess gene expression states of co-cultivated cells in response to tumor cells. *Mol. Cancer* **3**, 24. doi:10.1186/1476-4598-3-24
- Pernice, H. F., Schieweck, R., Jafari, M., Straub, T., Bilban, M., Kiebler, M. A. and Popper, B. (2019). Altered glutamate receptor ionotropic delta subunit 2 expression in Stau2-deficient cerebellar purkinje cells in the adult brain. *Int. J. Mol. Sci.* **20**, 1797. doi:10.3390/ijms20071797
- Petryniak, M. A., Potter, G. B., Rowitch, D. H. and Rubenstein, J. L. R. (2007). Dlx1 and Dlx2 control neuronal versus oligodendroglial cell fate acquisition in the developing forebrain. *Neuron* **55**, 417-433. doi:10.1016/j.neuron.2007.06.036
- Popper, B., Demleitner, A., Bolivar, V. J., Kusek, G., Snyder-Keller, A., Schieweck, R., Temple, S. and Kiebler, M. A. (2018). Staufen2 deficiency leads to impaired response to novelty in mice. *Neurobiol. Learn. Mem.* **150**, 107-115. doi:10.1016/j.nlm.2018.02.027
- Qian, X., Goderie, S. K., Shen, Q., Stern, J. H. and Temple, S. (1998). Intrinsic programs of patterned cell lineages in isolated vertebrate CNS ventricular zone cells. *Development* **125**, 3143-3152. doi:10.1242/dev.125.16.3143
- Rivero, O., Sich, S., Popp, S., Schmitt, A., Franke, B. and Lesch, K.-P. (2013). Impact of the ADHD-susceptibility gene CDH13 on development and function of brain networks. *Eur. Neuropsychopharmacol.* **23**, 492-507. doi:10.1016/j.euroneuro.2012.06.009
- Rosenberg, A. B., Roco, C. M., Muscat, R. A., Kuchina, A., Sample, P., Yao, Z., Graybuck, L. T., Peeler, D. J., Mukherjee, S., Chen, W. et al. (2018). Single-cell profiling of the developing mouse brain and spinal cord with split-pool barcoding. *Science (80- )* **360**, 176-182. doi:10.1126/science.aam8999
- Schwartz, N. B. and Domowicz, M. S. (2018). Proteoglycans in brain development and pathogenesis. *FEBS Lett.* **592**, 3791-3805. doi:10.1002/1873-3468.13026
- Sephton, C. F., Cenik, C., Kucukural, A., Dammer, E. B., Cenik, B., Han, Y., Dewey, C. M., Roth, F. P., Herz, J., Peng, J. et al. (2011). Identification of neuronal RNA targets of TDP-43-containing ribonucleoprotein complexes. *J. Biol. Chem.* **286**, 1204-1215. doi:10.1074/jbc.M110.190884
- Sessa, A., Mao, C., Hadjantonakis, A.-K., Klein, W. H. and Broccoli, V. (2008). Tbr2 directs conversion of radial glia into basal precursors and guides neuronal amplification by indirect neurogenesis in the developing neocortex. *Neuron* **60**, 56-69. doi:10.1016/j.neuron.2008.09.028
- Shen, Q., Wang, Y., Dimos, J. T., Fasano, C. A., Phoenix, T. N., Lemischka, I. R., Ivanova, N. B., Stifani, S., Morrissey, E. E. and Temple, S. (2006). The timing of cortical neurogenesis is encoded within lineages of individual progenitor cells. *Nat. Neurosci.* **9**, 743-751. doi:10.1038/nn1694
- Südhof, T. C. (2008). Neuroligins and neuexins link synaptic function to cognitive disease. *Nature* **455**, 903-911. doi:10.1038/nature07456
- Sugitani, Y., Nakai, S., Minowa, O., Nishi, M., Jishage, K.-I., Kawano, H., Mori, K., Ogawa, M. and Noda, T. (2002). Brn-1 and Brn-2 share crucial roles in the production and positioning of mouse neocortical neurons. *Genes Dev.* **16**, 1760-1765. doi:10.1101/gad.978002
- Tasic, B., Yao, Z., Graybuck, L. T., Smith, K. A., Nguyen, T. N., Bertagnoli, D., Goldy, J., Garren, E., Economo, M. N., Viswanathan, S. et al. (2018). Shared and distinct transcriptomic cell types across neocortical areas. *Nature* **563**, 72-78. doi:10.1038/s41586-018-0654-5
- Tawamie, H., Martianov, I., Wohlfahrt, N., Buchert, R., Mengus, G., Uebe, S., Janiri, L., Hirsch, F. W., Schumacher, J., Ferrazzi, F. et al. (2017). Hypomorphic pathogenic variants in TAF13 are associated with autosomal-recessive intellectual disability and microcephaly. *Am. J. Hum. Genet.* **100**, 555-561. doi:10.1016/j.ajhg.2017.01.032
- Tenenbaum, S. A., Lager, P. J., Carson, C. C. and Keene, J. D. (2002). Ribonomics: identifying mRNA subsets in mRNP complexes using antibodies to RNA-binding proteins and genomic arrays. *Methods* **26**, 191-198. doi:10.1016/S1046-2023(02)00022-1
- Ule, J., Jensen, K. B., Ruggiu, M., Mele, A., Ule, A. and Darnell, R. B. (2003). CLIP identifies Nova-regulated RNA networks in the brain. *Science* **302**, 1212-1215. doi:10.1126/science.1090095
- Vandoorne, T., De Bock, K. and Van Den Bosch, L. (2018). Energy metabolism in ALS: an underappreciated opportunity? *Acta Neuropathol.* **135**, 489-509. doi:10.1007/s00401-018-1835-x
- Vasitha, N. A., García-Moreno, F., Arora, S., Cheung, A. F. P., Arnold, S. J., Robertson, E. J. and Molnár, Z. (2015). Cortical and clonal contribution of Tbr2 expressing progenitors in the developing mouse brain. *Cereb. Cortex* **25**, 3290-3302. doi:10.1093/cercor/bhu125
- Vessey, J. P., Amadei, G., Burns, S. E., Kiebler, M. A., Kaplan, D. R. and Miller, F. D. (2012). An asymmetrically localized Staufen2-dependent RNA complex regulates maintenance of mammalian neural stem cells. *Cell Stem Cell* **11**, 517-528. doi:10.1016/j.stem.2012.06.010
- Wang, H., Farhan, M., Xu, J., Lazarovici, P. and Zheng, W. (2017). The involvement of DARPP-32 in the pathophysiology of schizophrenia. *Oncotarget* **8**, 53791-53803. doi:10.18632/oncotarget.17339
- Wang, Y., Ye, M., Kuang, X., Li, Y. and Hu, S. (2018). A simplified morphological classification scheme for pyramidal cells in six layers of primary somatosensory cortex of juvenile rats. *IBRO reports* **5**, 74-90. doi:10.1016/j.ibror.2018.10.001
- Wang, W., Zhao, F., Ma, X., Perry, G. and Zhu, X. (2020). Mitochondria dysfunction in the pathogenesis of Alzheimer's disease: recent advances. *Mol. Neurodegener.* **15**, 30. doi:10.1186/s13024-020-00376-6
- Watanabe, N., Kageyama, R. and Ohtsuka, T. (2015). Hbp1 regulates the timing of neuronal differentiation during cortical development by controlling cell cycle progression. *Development* **142**, 2278-2290.
- Wickham, L., Duchaine, T., Luo, M., Nabi, I. R. and DesGroseillers, L. (1999). Mammalian staufen is a double-stranded-RNA- and tubulin-binding protein which localizes to the rough endoplasmic reticulum. *Mol. Cell. Biol.* **19**, 2220-2230. doi:10.1128/MCB.19.3.2220
- Yeo, G. W., Coufal, N. G., Liang, T. Y., Peng, G. E., Fu, X.-D. and Gage, F. H. (2009). An RNA code for the FOX2 splicing regulator revealed by mapping RNA-protein interactions in stem cells. *Nat. Struct. Mol. Biol.* **16**, 130-137. doi:10.1038/nsmb.1545
- Zhao, J., Ohsumi, T. K., Kung, J. T., Ogawa, Y., Grau, D. J., Sarma, K., Song, J. J., Kingston, R. E., Borowsky, M. and Lee, J. T. (2010). Genome-wide identification of polycomb-associated RNAs by RIP-seq. *Mol. Cell* **40**, 939-953. doi:10.1016/j.molcel.2010.12.011
- Zhou, B., Osinski, J. M., Mateo, J. L., Martynoga, B., Sim, F. J., Campbell, C. E., Guillemot, F., Piper, M. and Gronostajski, R. M. (2015). Loss of NFIX transcription factor biases postnatal neural stem/progenitor cells toward oligodendrogenesis. *Stem Cells Dev.* **24**, 2114-2126. doi:10.1089/scd.2015.0136
- Zeisel, A., Muñoz-Manchado, A. B., Codeluppi, S., Lönnerberg, P., La Manno, G., Jureus, A., Marques, S., Munguba, H., He, L., Betsholtz, C. et al. (2015). Cell types in the mouse cortex and hippocampus revealed by single-cell RNA-seq. *Science (80- )* **347**, 1138-1142. doi:10.1126/science.aaa1934
- Zhang, Y., Chen, K., Sloan, S. A., Bennett, M. L., Scholze, A. R., O'Keefe, S., Phatnani, H. P., Guarnieri, P., Caneda, C., Ruderisch, N. et al. (2014). An RNA-sequencing transcriptome and splicing database of glia, neurons, and vascular cells of the cerebral cortex. *J. Neurosci.* **34**, 11929-11947. doi:10.1523/JNEUROSCI.1860-14.2014

## Supplementary information

### Materials and Methods

#### Enrichment analysis

Gene Ontology (GO) and REACTOME enrichment analyses were performed using the HypeR function (hypeR and msigdbR libraries) in R (see R code).

For the biological pathway (BP) enrichment analysis (Fig. 3C,D), LSAfun and rrvgo packages in R were used to reduce GO BP terms by identifying redundancy based on semantic similarity. Treemaps representing parent GO BP terms were made using the treemapify package in R (Fig. 3C,D). GGPlot2 was used to plot the top 10 enriched parent terms associated with genes maximally bound at E11.5, E13.5, E15.5 and E17.5 were plotted.

For parent pathway enrichment analyses (Fig. S3, Fig. 5E), the complete list of pathways (Table S13a) was downloaded from the REACTOME database, along with a pathway hierarchy relationship file that contained columns with REACTOME parent pathway (top tier) and child pathway (second or third tier) identifiers (Table S13b). From the complete list of pathways (Table S13a), we then identified pathways associated only with mouse genes. Next, we used the REACTOME pathways enriched for dynamic, partially dynamic and stable genes to identify the corresponding parent pathways in R (Table S13b). This produced a list of parent pathways for each category (dynamic, partially dynamic, and stable). Enriched parent pathways were then plotted using GGPlot2 in R. A similar method was used for maximally bound genes at each timepoint (Fig. 3F) and DL-STAU2 cargo vs not cargo genes (Fig. 5E).

#### Comparisons with published datasets

Genes in STAU2 cargo were compared to pro-IPC (ON) and non-IPC (OFF) gene lists generated by Aprea et al., 2012 and overlapping genes were identified using the inner\_join function (dplyr library) in R (Fig. 4C,D). Heatmaps showing the average

expression of these genes across the four time points were generated using the heatmap.2 function in R. Weighted mean expressions were calculated by applying peak scores as weights to read counts at each timepoint. This allowed us to quantify mean binding of STAU2 to cargo genes across the different captured regions. Weighted mean expressions of STAU2 cargo genes were used for this analysis.

Similarly, VZ, SVZ, and CP gene lists were obtained from the Fietz et al., 2013 study. STAU2 cargo genes were compared to these gene lists as described above and lists of overlapping genes were (GZ-Cargo) obtained. Markers present in genelists but not present in STAU2 cargo were designated GZ-Not Cargo. To obtain the DNA-binding (DB) genes, these overlapping genes were further filtered based on the 'transcription DNA-templated' term (GO:0006351) in the Gene Ontology (GO) database using the 'get\_anno\_genes' function (GofuncR library) in R. Heatmaps representing this data were generated as described above (Fig. 5A, S5B). Weighted mean expressions of STAU2 cargo genes were used for this analysis.

For phenotypic enrichment analysis, the DB gene lists obtained above were analyzed using the Mouse Genome Informatics (MGI) database (<http://www.informatics.jax.org/batch>) (Bult et al. 2019), and Mammalian Phenotype Ontology Enrichment (Smith & Eppig 2009) was determined through the MouseMine portal (Motenko et al. 2015). Graphs based on this data were generated in R (Fig. 5B,C).

For layer marker analysis, calibrated probabilities of genes enriched in cortical layers II-III, layer IV, layer V, layer VI and layer VIb were obtained from Belgard et al. 2011. Mean probabilities for layers II/III/IV (upper layer (UL)) and V/VI/VIb (deep layer (DL)) were determined. Probability values were scaled using the empirical cumulative distribution function (ECDF) function in R. Genes with mean scaled probabilities >0.9 were selected. Unique genes in each group were categorized as UL or DL markers. The cumulative expression of STAU2-bound layer markers was analyzed using a weighted means approach. Weights, ie. scaled probabilities of genes being specific for UL or DL, were used to calculate the weighted mean expression of UL and DL markers in the

cargo at the four timepoints. A line graph with a 90% confidence interval was generated showing the mean layer marker expression in STAU2 cargo (Fig. 5D).

#### Analysis of endothelial cell markers in the cargo

To assess whether there was significant post-lysis binding, we assessed STAU2 expression in a single cell dataset (Loo et al., 2019), and found that expression in endothelial cells (ECs) is much lower than other cell types at E14.5 in mouse. However, other studies indicate STAU2 is expressed in ECs in single cells derived from developing mouse brains and spinal cords (P2 and P11) (Rosenberg et al., 2018) and adult mouse brain ((Zhang et al., 2014)- <https://www.brainrnaseq.org/>, (Zeisel et al., 2015)- <http://linnarssonlab.org/cortex/>). Nevertheless, given the relatively low EC expression we rationalized that if there was extensive post-lysis binding this would be reflected in high EC transcript presence in the STAU2 cargo.

Using a database of mouse EC markers enriched over whole brain (Daneman et al., 2010), we evaluated the top 100 genes most highly enriched in ECs and found only 7 present in the cargo. Most common EC markers such as *Pecam1*, *Pglyrp1*, *Tie1*, *Epas1*, *Flt1* and *Fli1* were absent from our dataset, and just two specific EC markers, *Tek* and *Kdr* were present. As STAU2 may be expressed at a low level in ECs, we cannot rule out the possibility that STAU2 is genuinely binding these RNAs in ECs. Taken together, these observations are consistent with negligible post-lysis binding captured in the dataset.

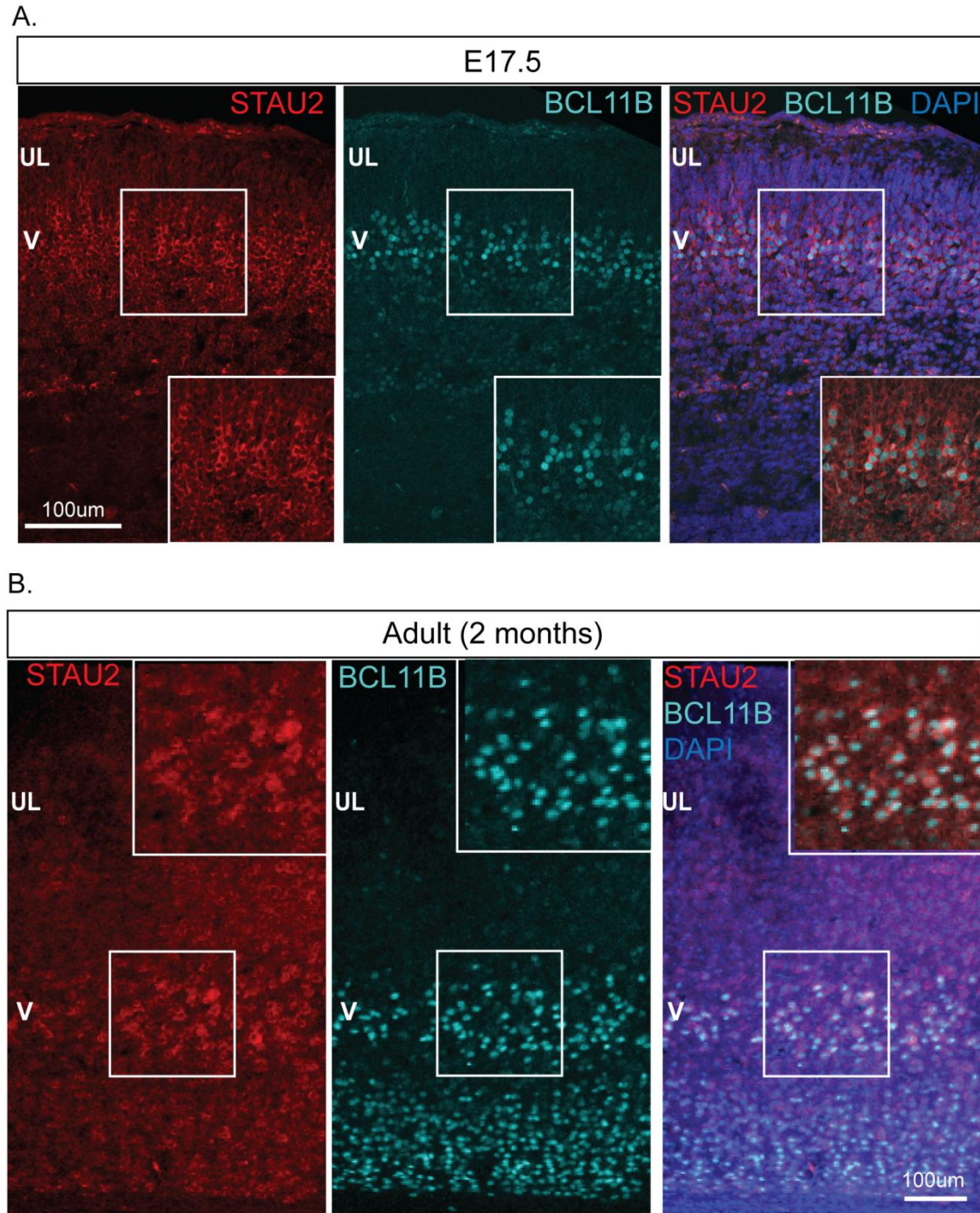
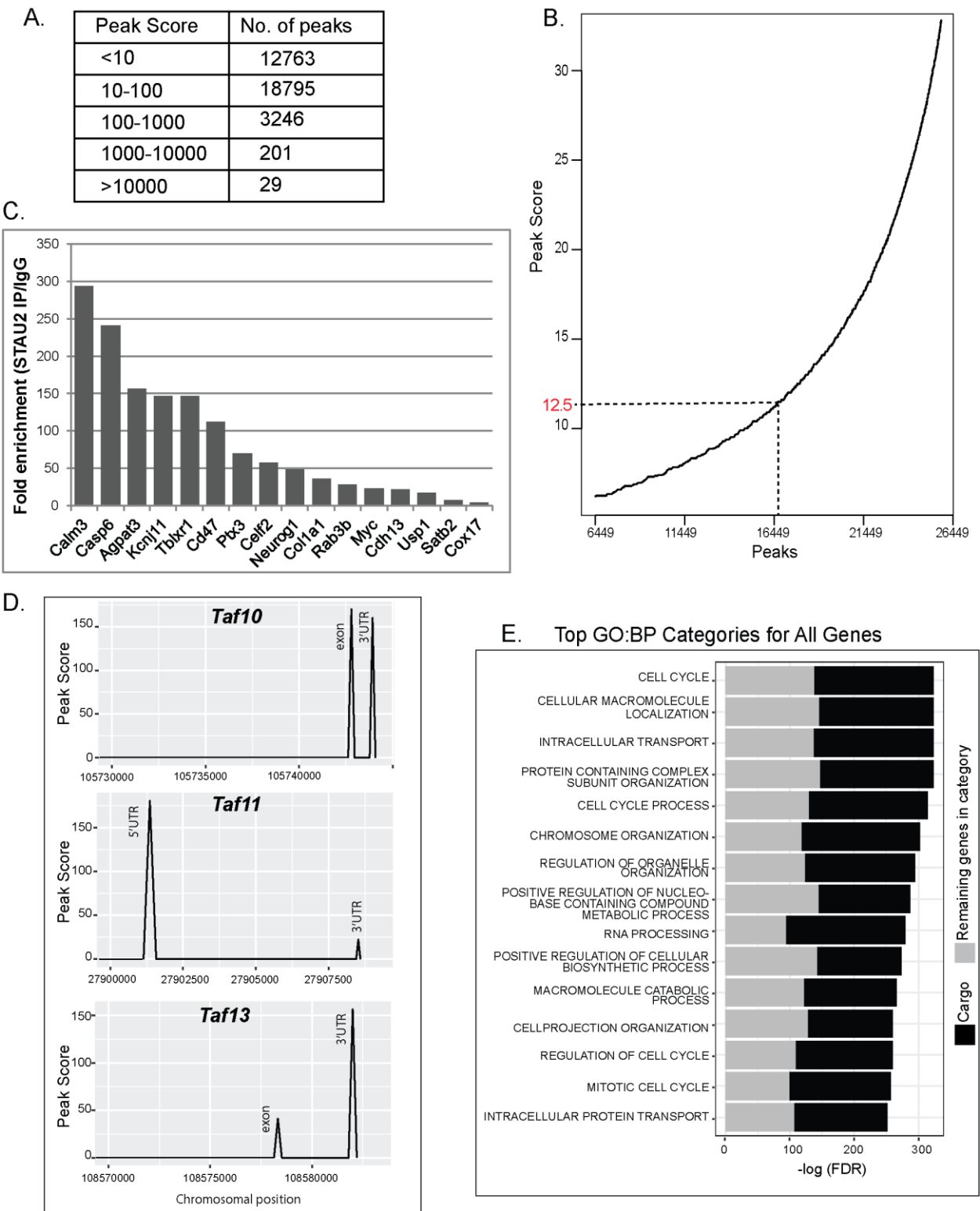


**Fig. S1.** (relates to Fig. 1). STAU2 is strongly expressed in BCL11B+ layer V cells in the developing and adult cortex. Immunohistochemistry using a STAU2-specific mouse monoclonal antibody in coronal sections revealed co-expression of STAU2 and BCL11B (CTIP2) at E17.5 (A) and 2 months (B). Scale bars= 100 µm.



the Y-axis. The elbow point (dotted lines) was determined to be 12.5 and this was set as peak score cut-off to determine the most enriched peaks. (C) qRT-PCR was used to validate presence of candidate genes in STAU2 RIPs over negative control IgG at E15.5. (D) Depiction of the transcript regions captured for representative genes, *Taf10*, *Taf11* and *Taf13*. Peaks observed corresponded to exon and 3'UTR for *Taf10*, 5'UTR and 3'UTR for *Taf11*, and exon and 3'UTR for *Taf13*. (E) The top 15 GO BP categories associated with all transcripts in STAU2 cargo. To illustrate the contribution of STAU2 cargo to each category, the bars are filled to show the proportion of STAU2 cargo (black) versus the remaining genes in the category (grey).



**Fig. S3.** (relates to Fig. 3). Balloon plot showing enriched REACTOME parent, ie. the top tier and the second-tier pathways associated with dynamic, partially dynamic and stable genes in STAU2 cargo. Color in the legend refers to the stability and percent is indicated by dot size. Percent refers to the contribution of the specified category to all the enriched categories for that particular stability group. Parent pathways corresponding to at least one percent of all enriched pathways are shown. Parent pathways higher in the dynamic group are indicated in red text, those enriched in the partially dynamic group are highlighted in green text, and those higher in the stable group are in blue text.

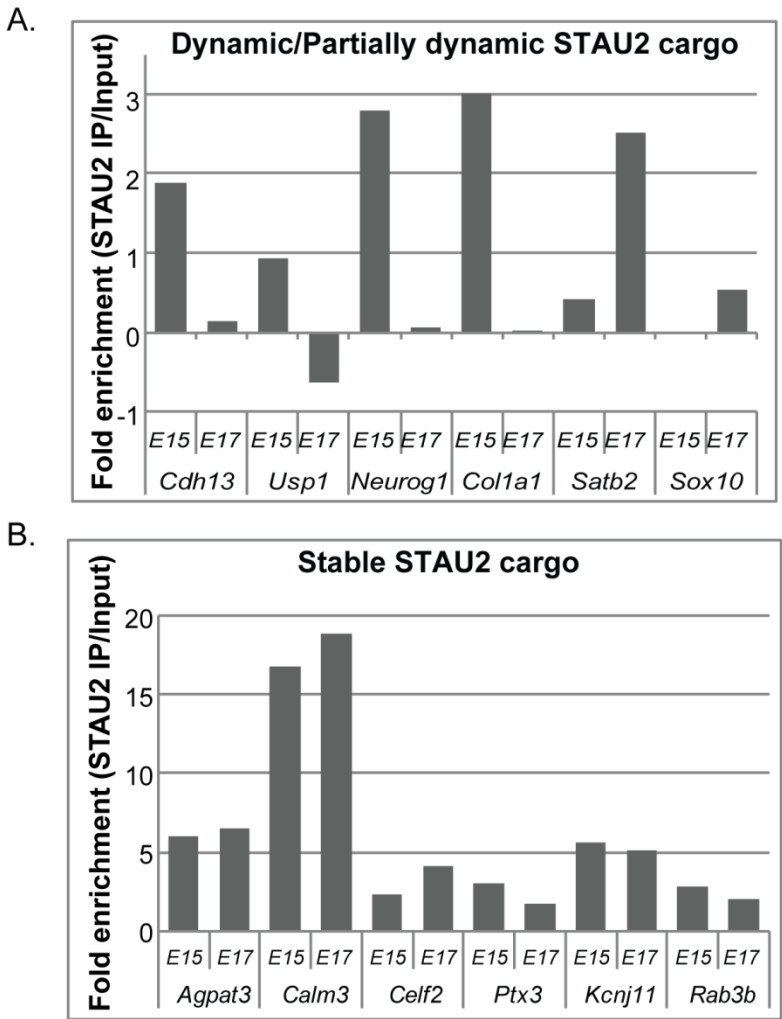


**Fig. S4.** (relates to Fig. 4). (A) qRT-PCR was used to validate presence of candidate genes in STAU2 RIPs over negative control IgG at E15.5. (B, C) Validation of dynamic and partially dynamic STAU2 cargo genes, *Cdh13*, *Usp1*, *Neurog1*, *Col1a1* and *Satb2* and stable STAU2 cargo genes, *Agpat3*, *Calm3*, *Celf2*, *Ptx3*, *Kcnj11* and *Rab3b* in RNA isolated from STAU2 RIPs using E15.5 and E17.5 mouse cortical tissue. Y-axis represents fold enrichment in STAU2 IP over input.

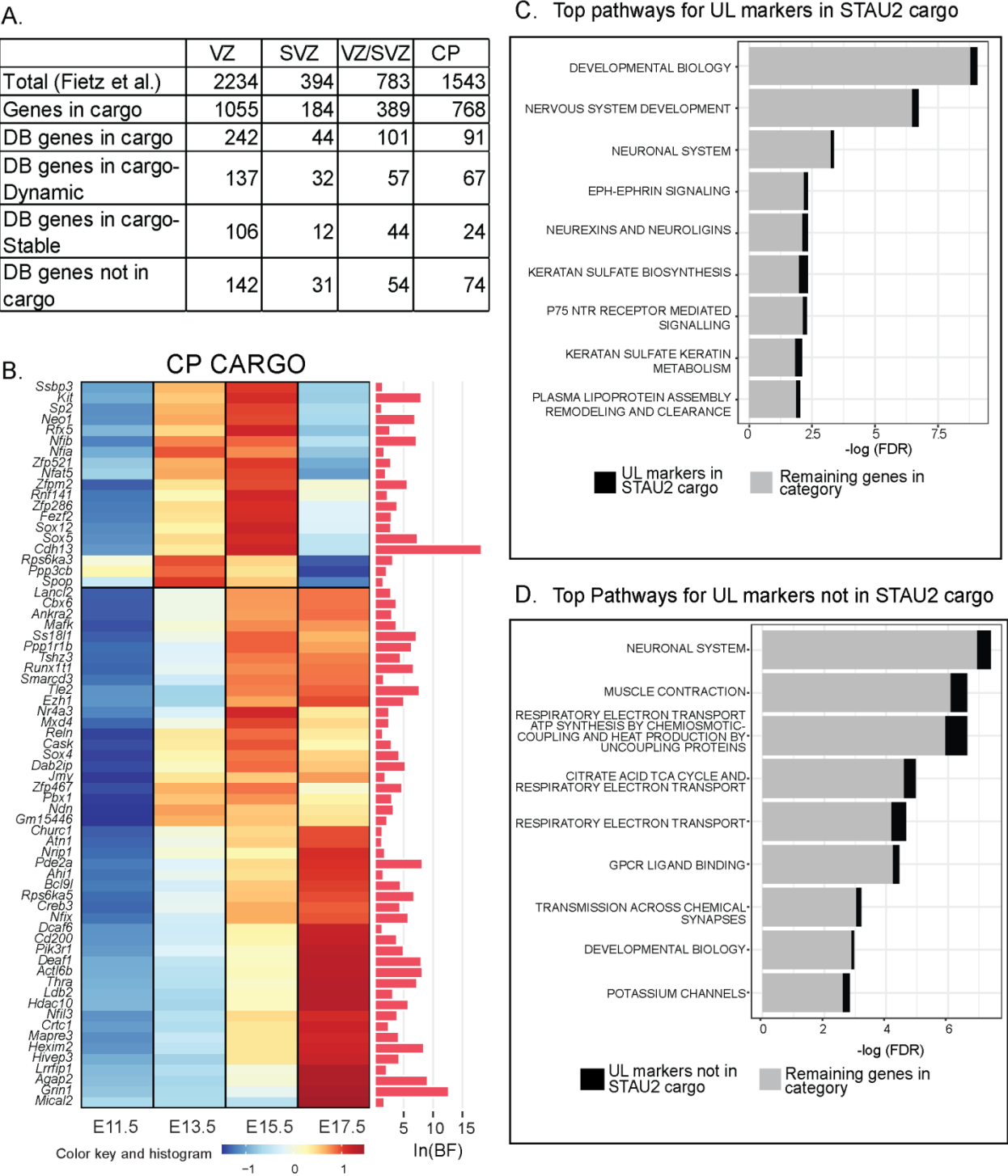


**Fig. S5.** (relates to Fig. 5). Comparison of STAU2 cargo with published datasets. Quantification of VZ, SVZ, VZ-SVZ and CP genes identified by Fietz et al., 2012, those present in the cargo, and DNA-binding genes in cargo and not in cargo for each zone. (B) Heatmap showing the average expression of dynamic and partially dynamic

CP-DB genes in the STAU2 cargo from E11.5 to E17.5. The horizontal bar graph on the right of the heatmap represents  $\ln(\text{BF})$ . Color key represents z-score after scaling across rows, with red signifying higher expression and purple signifying lower expression. (C) The top REACTOME pathways differentially enriched for UL transcripts in STAU2 cargo. (D) The top enriched REACTOME pathways for transcripts identified as UL markers that were not present in STAU2 cargo. To illustrate the contribution of STAU2 cargo to each category, the bars are filled to show the proportion of STAU2 cargo or not cargo genes (black) versus the remaining genes in the category (grey).

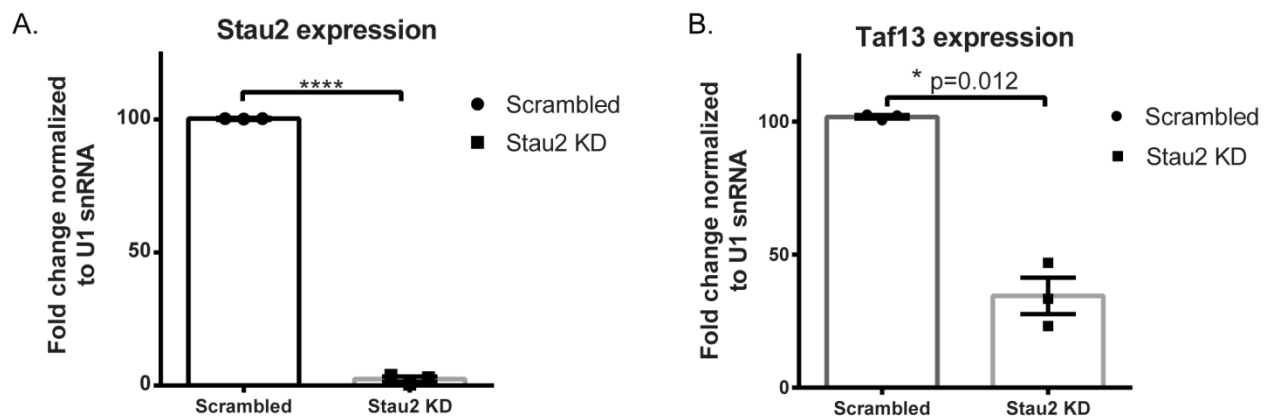


**Fig. S6.** (relates to Fig. 6). Knockdown of *Stau2* leads to a reduction in *Taf13* expression. E12.5 mouse cortices were dissected, dissociated, and infected with scrambled shRNA as control or shRNAs targeting *Stau2* at MOI=3, and cultured for 3 DIV. qRT-PCR was used to quantify the reduction of *Stau2* (A), and *Taf13* (B) expression. Fold change in expression was normalized to U1 snRNA. \*p < 0.05, paired student's t test, n=3. Graphs show means $\pm$ SEM.

**Table S1.** STAU2 RIP-seq peaks file with count data

[Click here to download Table S1](#)

**Table S2.** Pairwise comparison of  $\ln(\text{BF})$ s assigned to STAU2 cargo genes at different time points and summed  $\ln(\text{BF})$ .

[Click here to download Table S2](#)

**Table S3.** GO biological process (BP) and REACTOME pathway enrichment of all STAU2 cargo.

- a) List of GO biological processes (BP) associated with all STAU2 cargo genes.
- b) List of REACTOME pathways associated with all STAU2 cargo genes.

For all GO BP and pathways enrichment analyses, 'signature' refers to total genes analyzed, 'geneset' refers to the total number of genes associated with the category, and 'overlap' refers to the number of genes in the cargo that match the geneset.

[Click here to download Table S3](#)

**Table S4.** GO biological process (BP) and REACTOME pathway enrichment of dynamic STAU2 cargo.

- a) List of GO biological processes (BP) associated with dynamic STAU2 cargo genes.
- b) List of REACTOME pathways associated with dynamic STAU2 cargo genes.
- c) Parent BP terms for dynamic STAU2 cargo genes (treemap data)

[Click here to download Table S4](#)

**Table S5.** GO biological process (BP) and REACTOME pathway enrichment of partially dynamic STAU2 cargo.

- a) List of GO biological processes (BP) associated with partially dynamic STAU2 cargo genes.
- b) List of REACTOME pathways associated with partially dynamic STAU2 cargo genes.
- c) Parent BP terms for partially dynamic STAU2 cargo genes (treemap data)

[Click here to download Table S5](#)

**Table S6.** GO biological process (BP) and REACTOME pathway enrichment of stable STAU2 cargo.

- a) List of GO biological processes (BP) associated with stable STAU2 cargo genes.
- b) List of REACTOME pathways associated with stable STAU2 cargo genes.
- c) Parent BP terms for stable STAU2 cargo genes (treemap data)

[Click here to download Table S6](#)

**Table S7.** REACTOME parent pathways associated with dynamic, partially dynamic and strongly stable STAU2 cargo.

- a) List of REACTOME parent pathways associated with dynamic STAU2 cargo genes.
- b) List of REACTOME parent pathways associated with partially dynamic STAU2 cargo genes.
- c) List of REACTOME parent pathways associated with stable STAU2 cargo genes.
- d) Table showing the percentage of contribution of a particular category to all enriched REACTOME parent categories for dynamic, partially dynamic and strongly stable STAU2 cargo pathways.

[Click here to download Table S7](#)

**Table S8.** Parent GO biological process (BP) enrichment of STAU2 cargo genes maximally bound at E11.5, E13.5, E15.5 and E17.5.

- a) List of GO BO terms and parent terms associated with genes maximally bound at E11.5.
- b) List of GO BO terms and parent terms associated with genes maximally bound at E12.5.
- c) List of GO BO terms and parent terms associated with genes maximally bound at E13.5.
- d) List of GO BO terms and parent terms associated with genes maximally bound at E17.5.
- e) Table showing the percentage of contribution of a particular category to top 10 enriched parent categories for STAU2 cargo with highest binding at each time point.
- f) Lists of genes with maximum binding at each time point.

[Click here to download Table S8](#)

**Table S9.** Pro-IPC and Non-IPC genes in cargo

- a) Read counts and summed ln(BF)s of pro-IPC genes in STAU2 cargo.
- b) Read counts and summed ln(BF)s of non-IPC genes in STAU2 cargo.

[Click here to download Table S9](#)

**Table S10.** Phenotypic enrichment of VZ-DB, SVZ-DB and CP-DB genes

- a) Gene lists corresponding to VZ, SVZ, VZ-SVZ, CP DNA-binding (DB) genes in present cargo, stable and dynamic SVZ (SVZ+VZ-SVZ)-DB and VZ-DB genes in STAU2 cargo, and VZ, SVZ, VZ-SVZ, CP DB genes not in STAU2 cargo. Dynamic=dynamic and partially dynamic STAU2 cargo genes. Stable= stable and strongly stable STAU2 cargo genes.
- b) Mammalian Phenotype (MP) terms enriched for VZ-DB cargo and not cargo genes downloaded from the MouseMine portal.
- c) Mammalian Phenotype (MP) terms enriched for SVZ-DB cargo and not cargo genes downloaded from the MouseMine portal.
- d) Mammalian Phenotype (MP) terms enriched for VZ-SVZ-DB cargo and not cargo genes downloaded from the MouseMine portal.
- e) Mammalian Phenotype (MP) terms enriched for CP-DB cargo and not cargo genes downloaded from the MouseMine portal.
- f) Mammalian Phenotype (MP) terms enriched for dynamic+partially dynamic and stable VZ-DB and SVZ(VZ+VZ-SVZ)-DB cargo downloaded from the MouseMine portal.

[Click here to download Table S10](#)

**Table S11.** REACTOME pathway enrichment of deep layer (DL) and upper layer (UL) markers in STAU2 cargo and those not present in STAU2 cargo.

- a) List of REACTOME pathways associated with DL markers present in STAU2 cargo.
- b) List of REACTOME pathways associated with DL markers not present in STAU2 cargo.
- c) List of REACTOME parent pathways associated with DL markers present in STAU2 cargo.
- d) List of REACTOME parent pathways associated with DL markers not present in STAU2 cargo.
- e) Table showing the percentage of contribution of a particular category to all enriched REACTOME parent categories for DL STAU2 cargo and not cargo pathways.
- f) List of REACTOME pathways associated with UL markers present in STAU2 cargo.
- g) List of REACTOME pathways associated with UL markers not present in STAU2 cargo.
- h) Lists of UL and DL markers present in STAU2 cargo and those not present in cargo.

[Click here to download Table S11](#)

**Table S12.** Primary antibody, primer and shRNA information.

[Click here to download Table S12](#)

**Table S13.** REACTOME complete list of pathways

- a) A complete list of pathways downloaded from the REACTOME database.
- b) Pathway hierarchy relationship file downloaded from the REACTOME database containing REACTOME parent pathway (top tier) and child pathway (second or third tier) identifiers.

[Click here to download Table S13](#)

## References

- Bult, C.J. et al., 2019. Mouse Genome Database (MGD) 2019. *Nucleic acids research*, 47(D1), pp.D801–D806.
- Daneman, R., Zhou, L., Agalliu, D., Cahoy, J. D., Kaushal, A. and Barres, B. A. (2010). The Mouse Blood-Brain Barrier Transcriptome: A New Resource for Understanding the Development and Function of Brain Endothelial Cells. *PLoS One* 5, e13741.
- Loo, L., Simon, J. M., Xing, L., McCoy, E. S., Niehaus, J. K., Guo, J., Anton, E. S. and Zylka, M. J. (2019). Single-cell transcriptomic analysis of mouse neocortical development. *Nat. Commun.* 10, 134.
- Motenko, H. et al., 2015. MouseMine: a new data warehouse for MGI. *Mammalian genome : official journal of the International Mammalian Genome Society*, 26(7–8), pp.325–330.
- Rosenberg, A. B., Roco, C. M., Muscat, R. A., Kuchina, A., Sample, P., Yao, Z., Graybuck, L. T., Peeler, D. J., Mukherjee, S., Chen, W., et al. (2018). Single-cell profiling of the developing mouse brain and spinal cord with split-pool barcoding. *Science* (80-. ). 360, 176 LP-182.
- Smith, C.L. & Eppig, J.T., 2009. The mammalian phenotype ontology: enabling robust annotation and comparative analysis. *Wiley interdisciplinary reviews. Systems biology and medicine*, 1(3), pp.390–399.
- Zeisel, A., Muñoz-Manchado, A. B., Codeluppi, S., Lönnerberg, P., La Manno, G., Juréus, A., Marques, S., Munguba, H., He, L., Betsholtz, C., et al. (2015). Cell types in the mouse cortex and hippocampus revealed by single-cell RNA-seq. *Science* (80-. ). 347, 1138 LP-1142.
- Zhang, Y., Chen, K., Sloan, S. A., Bennett, M. L., Scholze, A. R., O’Keefe, S., Phatnani, H. P., Guarnieri, P., Caneda, C., Ruderisch, N., et al. (2014). An RNA-Sequencing Transcriptome and Splicing Database of Glia, Neurons, and Vascular Cells of the Cerebral Cortex. *J. Neurosci.* 34, 11929 LP-11947.